

Thermodynamic Inference in Partially Accessible Markov Networks: A Unifying Perspective from Transition-Based Waiting Time Distributions

Jann van der Meer[✉], Benjamin Ertel[✉], and Udo Seifert[✉]

II. Institut für Theoretische Physik, Universität Stuttgart, 70550 Stuttgart, Germany

 (Received 22 March 2022; revised 2 June 2022; accepted 1 July 2022; published 12 August 2022)

The inference of thermodynamic quantities from the description of an only partially accessible physical system is a central challenge in stochastic thermodynamics. A common approach is coarse-graining, which maps the dynamics of such a system to a reduced effective one. While coarse-graining states of the system into compound ones is a well-studied concept, recent evidence hints at a complementary description by considering observable transitions and waiting times. In this work, we consider waiting time distributions between two consecutive transitions of a partially observable Markov network. We formulate an entropy estimator using their ratios to quantify irreversibility. Depending on the complexity of the underlying network, we formulate criteria to infer whether the entropy estimator recovers the full physical entropy production or whether it just provides a lower bound that improves on established results. This conceptual approach, which is based on the irreversibility of underlying cycles, additionally enables us to derive estimators for the topology of the network, i.e., the presence of a hidden cycle, its number of states, and its driving affinity. Adopting an equivalent semi-Markov description, our results can be condensed into a fluctuation theorem for the corresponding semi-Markov process. This mathematical perspective provides a unifying framework for the entropy estimators considered here and established earlier ones. The crucial role of the correct version of time reversal helps to clarify a recent debate on the meaning of formal versus physical irreversibility. Extensive numerical calculations based on a direct evaluation of waiting time distributions illustrate our exact results and provide an estimate on the quality of the bounds for affinities of hidden cycles.

DOI: [10.1103/PhysRevX.12.031025](https://doi.org/10.1103/PhysRevX.12.031025)

Subject Areas: Statistical Physics

I. INTRODUCTION

Over the past two decades, stochastic thermodynamics has emerged as a comprehensive universal framework for describing small driven systems [1–5]. One major paradigm comprises a Markovian, i.e., memoryless, dynamics on a set of discrete states, which arises from integrating out fast microscopic degrees of freedom under the assumption of a timescale separation. Such a fairly general Markov network model is of widespread use in the description of chemical and biophysical processes, ranging from chemical reaction networks [6–10] to protein folding [11–13], molecular motors [14–19], and molecular dynamics in general [20–22].

There is, however, a difference between identifying an effective description of a complex system and actually having full access to it in practice. On the arguably coarsest level of description, one is interested in estimation methods

of crucial quantities like the entropy production. As a prominent result, the thermodynamic uncertainty relation (TUR) [23–25] provides thermodynamic bounds that can be used in estimation techniques for entropy [26–31] or topology [32,33] if it is possible to measure currents of the underlying system. These currents are a trace of the fundamental time-reversal asymmetry in dissipative systems [34,35] that can also be utilized directly as an entropy estimator [36–38]. Furthermore, entropy estimators that incorporate or are even based on waiting times between measurable events have been discussed more recently [39–42]. For a partially visible Markov network, entropy production can be estimated through the fraction that is visible in the subsystem through passive observation [43] or by controlling adjustable parameters [44,45].

These methods raise the general issue how an underlying, only partially accessible system is related to a reduced effective model, a topic known as coarse-graining in stochastic thermodynamics. Earlier interest in the field mainly considered coarse-graining as a mapping in which unresolved Markov states are lumped into compound states, for example, via schemes described in Refs. [46–50]. In general, the resulting system is no longer Markovian, so that a description of the dynamics or the entropy production is

Published by the American Physical Society under the terms of the Creative Commons Attribution 4.0 International license. Further distribution of this work must maintain attribution to the author(s) and the published article's title, journal citation, and DOI.

formulated in terms of phenomenological, apparent equations [27,51–55]. While particular symmetric systems can be described as semi-Markov processes in this coarse-graining approach [56–58], a general framework to describe situations with incomplete information remains an open issue. To give a recent example [59,60], allowing states that are not contained in any compound state breaks with the well-studied paradigm of state lumping as coarse-graining scheme. This novel scheme extends our ability to formulate thermodynamically consistent models while also exhibiting new effects such as kinetic hysteresis that require a refined understanding of the relationship between time reversal and coarse-graining.

In this work, we discuss thermodynamic inference based on the observation of a few transitions and their waiting time distributions rather than on the observation of a few states. This strategy has been proposed independently in the very recent Ref. [61], where the corresponding estimator for entropy production is introduced and its properties derived using mainly concepts from information theory, in particular, the Kullback-Leibler divergence. In our complementary approach that is based on the analysis of cycles, we show that the underlying trajectory-dependent quantity obeys a fluctuation theorem. Our analysis reveals that this estimator is the entropy production of a semi-Markov process. In particular, we show that the description discussed in the present work and in Ref. [61] shows kinetic hysteresis [59]. Mathematically, this effect is the consequence of a time-reversal operation that differs from the one that is usually employed for semi-Markov processes. In this context, higher-order semi-Markov processes [39] fit into the picture naturally as semi-Markov processes with yet another time-reversal operation. Thus, our mathematical perspective establishes semi-Markov processes as an underlying common model while also highlighting the subtleties involved in identifying the correct time-reversal operation.

Thermodynamic inference is not limited to estimating entropy production. We show that the waiting time distributions allow us to infer topological properties and further thermodynamic quantities like the number of states in cycles and their driving affinity. Furthermore, we propose an inductive scheme to detect the presence of hidden cycles in a complex network.

The paper is structured as follows. In Sec. II, we describe the setup and present our key results qualitatively. The fundamental concepts of our effective description are introduced in Sec. III for the paradigmatic model of a single observed link in a unicyclic Markov network. By generalizing these concepts to multicyclic Markov networks in Sec. IV, we propose and discuss an entropy estimator and inference methods theoretically and numerically. The general framework of multiple observed links in a multicyclic Markov network is discussed in Sec. V. In Sec. VI, we discuss our and related work from the perspective of semi-Markov processes. We conclude with a summary and an outlook on further work in Sec. VII.

II. SETUP AND KEY QUALITATIVE RESULTS

We start with a general Markov network of N interconnected states, e.g., the one shown in Fig. 1(a). At time t , a state $i(t) = k$ is assigned to the physical system, with $k = 1, \dots, N$. The time evolution follows a stochastic description by allowing transitions between two states k and l that are connected by a link (equivalently, an edge) in the network. Quantitatively, these transitions from k to l and their reverse happen instantaneously with transition rates k_{kl} and k_{lk} , respectively. We assume that $k_{kl} > 0$ implies $k_{lk} > 0$ to ensure thermodynamic consistency. In the long-time limit $t \rightarrow \infty$, the probability $p_k(t)$ to observe the system in a particular state k at time t approaches a constant value p_k^s , which characterizes the stationary state of the network.

In general networks, it is possible to walk along closed loops. These are accessed systematically from the network by identifying its cycles \mathcal{C} , which are defined as closed, directed loops without self-crossings. From a thermodynamic perspective, cycles are a crucial concept due to their possibility to break time-reversal symmetry by favoring the forward direction over the reverse or vice versa. This preference is quantified by the cycle affinity $\mathcal{A}_{\mathcal{C}}$, defined as the product over all forward rates in \mathcal{C} divided by the corresponding backward rates:

$$\mathcal{A}_{\mathcal{C}} = \ln \prod_{(kl) \in \mathcal{C}} \frac{k_{kl}}{k_{lk}}. \quad (1)$$

As shown in Fig. 1(b), the network from Fig. 1(a) has three different cycles with different affinities. The affinity $\mathcal{A}_{\mathcal{C}}$ is also related to the entropy production associated with the cycle \mathcal{C} [62,63]. For biochemical reactions or driving along a periodic track by a force, the affinity is given by the free energy change or dissipated work, respectively [3].

Cycles \mathcal{C} with nonvanishing affinities give rise to macroscopic, sustained flows along their constituent links, even in the limit of large observation times T . These circular flows are the cause of the mean entropy production rate

$$\langle \sigma \rangle = \sum_{\mathcal{C}} j_{\mathcal{C}} \mathcal{A}_{\mathcal{C}}, \quad (2)$$

where $j_{\mathcal{C}}$ is the expected net number of completed cycles \mathcal{C} divided by the observation time T in the limit $T \rightarrow \infty$ [63–65]. If $\langle \sigma \rangle > 0$, there is a constant rate of dissipation in the stationary state, which is then referred to as a nonequilibrium stationary state (NESS).

Calculating the entropy production via Eq. (2) requires the ideal case of knowing all cycles and all cycle currents, which is not practically feasible, in general. In our setup, we assume that an external observer measures individual transitions along a limited number of edges connecting neighboring states in the Markov network. Conceptually,

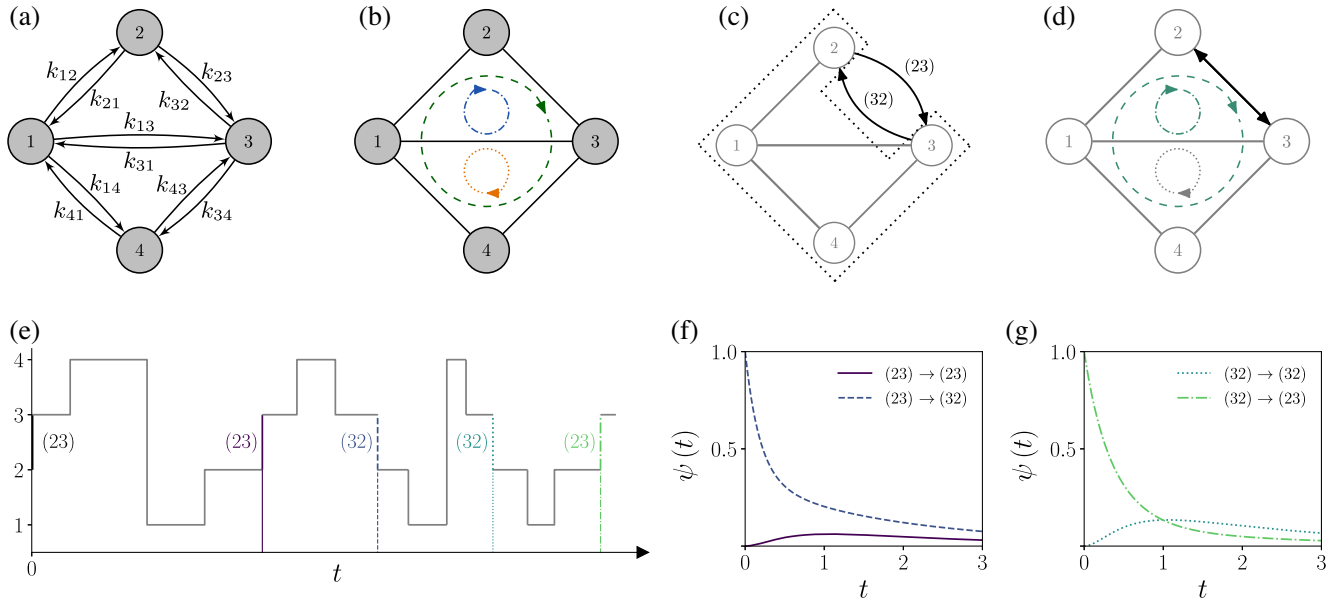


FIG. 1. Key concepts of the effective description for an exemplary Markov network. (a) Markov network including four different states. Every link between state i and state j allows for transitions in both directions with respective transition rates k_{ij} and k_{ji} . (b) Different cycles within the network. The three different cycles in the network are numbered incrementally starting with cycle $\mathcal{C}_0 = (12341)$, drawn as a green dashed curve, cycle $\mathcal{C}_1 = (1231)$, drawn as a blue dash-dotted curve, and cycle $\mathcal{C}_2 = (1341)$, drawn as an orange dotted curve. By definition in Eq. (1), the affinity of \mathcal{C}_0 is given by $\mathcal{A}_{\mathcal{C}_0} = \ln(k_{12}k_{23}k_{34}k_{41}/k_{21}k_{32}k_{43}k_{14})$; $\mathcal{A}_{\mathcal{C}_1}$ and $\mathcal{A}_{\mathcal{C}_2}$ are defined analogously. Furthermore, these affinities coincide with $\mathcal{A}_{\mathcal{C}} = \ln \mathcal{P}(\mathcal{C})/\mathcal{P}(\overline{\mathcal{C}})$, the quotient of probabilities to observe a completed cycle in the forward and backward direction, respectively [cf. Eq. (7)]. (c) Effective description of the network if only the link between 2 and 3 is observable. Observing this link gives information about transitions between 2 and 3, i.e., (23) and its reverse (32), and intermediate waiting times. (d) Observable cycles in the effective description. Two successive transitions along the observable link indicate the completion of a cycle. As indicated with gray color, only completions of \mathcal{C}_0 or \mathcal{C}_1 can be registered, since \mathcal{C}_2 does not include the observed link. Additionally, \mathcal{C}_0 and \mathcal{C}_1 are drawn as curves with the same color, because, by counting transitions without temporal resolution, we cannot distinguish between both cycles. (e) A trajectory and its effective description. The observable parts of a trajectory of the underlying network are transitions (23) and (32) at corresponding transition times. By conditioning the observed transitions on the previous ones, four different waiting time distributions for the different combinations of subsequent transitions can be defined. (f),(g) Waiting time distributions for the observable link for fixed transition rates. The four different waiting time distributions of the observed link are illustrated; they are calculated with the method introduced in Appendix A 3. The particular choice of transition rates is given in Appendix E.

this approach coincides with the transition-based effective description proposed in Ref. [61]. Notationally, we discern transitions from states by utilizing capital letters I, J, \dots and write $I = (kl)$ to express that I is a transition from the Markov state k to the Markov state l . An example illustrating this effective description for observable transitions (23) and (32) in the Markov network from Fig. 1(a) is shown in Figs. 1(c) and 1(d). The central objects of interest for this effective description are waiting time distributions of the form

$$\psi_{I \rightarrow J}(t) \equiv P(J; T_J - T_I = t | I), \quad (3)$$

which quantify the probability density that the transition J is measured at time $T_J = T_I + t$ given that the previous transition I is registered at time T_I . With transitions I, J replacing states k, l , waiting time distributions $\psi_{I \rightarrow J}(t)$ are the time-resolved analog of transition rates k_{kl} . Figures 1(e)–1(g) illustrate the concept of waiting time distributions for the effective description in Figs. 1(c)

and 1(d). In the following, we derive several remarkable results centered around these waiting time distributions and their underlying semi-Markov description, which are summarized here on a qualitative level.

- (1) For a unicyclic network, it is sufficient to determine the $\psi_{I \rightarrow J}(t)$ from just one edge in order to infer the affinity of the cycle \mathcal{C} and the exact mean entropy production rate $\langle \sigma \rangle$ from the ratio of these distributions. We recover this result of Ref. [61] independently, here based on a microscopic fluctuation theorem from the perspective of network cycles. Since the full entropy production is inferred by this estimator, it beats the TUR, which, in general, does not recover full entropy production even in a unicycle.
- (2) For a multicyclic network, the same information from just one edge yields the affinity of the shortest cycle, its length, and the length of the second-shortest cycle this edge is a part of. Second, it yields a lower bound on the largest cycle affinity contributing to the current through this edge. Finally, it

provides a lower bound on the overall entropy production of the network that coincides with the bound proposed in Ref. [61]. This bound is shown to be tighter than the entropy estimator in Ref. [44] while also omitting any assumptions of physical control over system parameters at the observed edge.

- (3) If several edges can be observed, the estimator on total entropy production becomes successively tighter. Based on the ratios of the $\psi_{I \rightarrow J}(t)$, we establish operational criteria to infer the presence of hidden cycles and hidden entropy production not accounted for by the estimator.
- (4) From a mathematical perspective, observing transitions results in a semi-Markov process. The cycle-based approach of this work and the information-theoretical approach of Ref. [61] can be seen as equivalent strategies to establish the entropy production of the corresponding semi-Markov process. From this point of view, we relate the proposed entropy estimator to the semi-Markov entropy estimator proposed and discussed in Refs. [39,66,67] and highlight the crucial role of the different time-reversal operations.

III. UNICYCLIC NETWORK AS PARADIGM

For an introductory example, we consider a Markov network with only a single cycle \mathcal{C} in its NESS. In this network, we observe a single edge between neighboring states k and l that is part of the cycle. We assume that forward and backward transitions along this edge can be distinguished and denote forward transitions (kl) as I_+ and backward transitions (lk) by I_- , respectively.

On the microscopic level, a waiting time distribution of the form $\psi_{I \rightarrow J}(t)$ has contributions only from microscopic trajectories $\gamma_{I \rightarrow J}^t$ that start with a transition I and end with another one, J , after time t without any other observed transition in between. With a microscopic path weight $\mathcal{P}[\gamma]$ for microscopic trajectories γ , the waiting time distribution can be expressed as

$$\psi_{I \rightarrow J}(t) = \sum_{\gamma_{I \rightarrow J}^t} \mathcal{P}[\gamma_{I \rightarrow J}^t | I], \quad (4)$$

which sums only trajectory snippets of the form $\gamma = \gamma_{I \rightarrow J}^t$ with a path weight that is conditioned on the first jump I at time T_I . For example, the waiting time distribution $\psi_{I_+ \rightarrow I_+}(t)$ originates from a trajectory snippet $\gamma_{I_+ \rightarrow I_+}^t$ of length t with the jump sequence $\gamma_{I_+ \rightarrow I_+}^t = k \rightarrow l \rightarrow \dots \rightarrow k \rightarrow l$. Likewise, $\psi_{I_- \rightarrow I_-}(t)$ arises from $\gamma_{I_- \rightarrow I_-}^t = l \rightarrow k \rightarrow \dots \rightarrow l \rightarrow k$. Although the identification in Eq. (4) is reasonable from a practical point of view, its derivation contains some subtleties that are explained in the full proof of Eq. (4) in Appendix A.

Since $\gamma_{I_- \rightarrow I_-}^t$ is the reverse of $\gamma_{I_+ \rightarrow I_+}^t$, the logarithmic ratio of the corresponding waiting time distributions,

$$a(t) \equiv a_{I_+ \rightarrow I_+}(t) \equiv \ln \frac{\psi_{I_+ \rightarrow I_+}(t)}{\psi_{I_- \rightarrow I_-}(t)}, \quad (5)$$

is a natural, antisymmetric measure of irreversibility of the underlying trajectory. As a first main result, we show that $a(t)$ is independent of t and, in particular, can be identified with the cycle affinity $\mathcal{A}_\mathcal{C}$:

$$a_{I_+ \rightarrow I_+}(t) \equiv a = -a_{I_- \rightarrow I_-}(t) = \mathcal{A}_\mathcal{C}. \quad (6)$$

This relation can be seen as a fluctuation theorem applied to sections of the underlying trajectory on the Markov network that give rise to a waiting time distribution $\psi_{I_+ \rightarrow I_+}(t)$. These sections are trajectory snippets $\gamma_{I_+ \rightarrow I_+}^t$ of the form given above, where the time difference between both jumps $k \rightarrow l$ is exactly t . To observe the genuine time reverse $\psi_{I_- \rightarrow I_-}(t)$, the underlying trajectory must complete the cycle in the reverse direction, which means

$$\mathcal{P}[\gamma_{I_- \rightarrow I_-}^t | I_-] = \mathcal{P}[\gamma_{I_+ \rightarrow I_+}^t | I_+] e^{-\mathcal{A}_\mathcal{C}} \quad (7)$$

for the path weights of every possible trajectory snippet $\gamma_{I_\pm \rightarrow I_\pm}^t$. Since this argument holds true for all trajectories contributing to the waiting time distribution $\psi_{I_+ \rightarrow I_+}(t)$, we can sum the left side of Eq. (7) over all $\gamma_{I_- \rightarrow I_-}^t$ and the right side of Eq. (7) over all $\gamma_{I_+ \rightarrow I_+}^t$ to conclude that

$$\psi_{I_- \rightarrow I_-}(t) = \psi_{I_+ \rightarrow I_+}(t) e^{-\mathcal{A}_\mathcal{C}} \quad (8)$$

using Eq. (4). Inserting Eq. (8) into Eq. (5) proves Eq. (6).

Since $a(t) = a = \mathcal{A}_\mathcal{C}$ is time independent, we get from Eq. (5) to

$$\mathcal{A}_\mathcal{C} = a = \ln \frac{\int_0^\infty dt \psi_{I_+ \rightarrow I_+}(t)}{\int_0^\infty dt \psi_{I_- \rightarrow I_-}(t)} = \ln \frac{P(I_+ | I_+)}{P(I_- | I_-)} \quad (9)$$

with an integration over the time t . The last equality follows from the definition of $\psi_{I \rightarrow J}(t)$ as a joint distribution in J and t in Eq. (3). Thus, the cycle affinity is encoded in conditional probabilities $P(J|I)$ to observe transition J after transition I irrespective of the intermediate waiting time. The relationship between cycle affinities and a time-antisymmetric probability ratio, given by Eq. (6) [or, equivalently, Eq. (9)], indicates that $a(t)$ can be used as an estimator for the mean entropy production rate $\langle \sigma \rangle$ in the steady state via

$$\langle \sigma \rangle = j_\mathcal{C} \mathcal{A}_\mathcal{C} = j_\mathcal{C} a, \quad (10)$$

which is exact even for finite observation times T , because the average is taken in the NESS. This noninvasive

estimator is directly accessible from an operational point of view, as by definition j_C can be calculated by counting transitions along the observed link and $a(t) = a$ can be calculated either directly from histogram data for the waiting time distributions using Eq. (5) or from conditional probabilities deduced from observed transitions using Eq. (9). This unicyclic result also recovers one of the main results in Ref. [61], here using a technique based on the microscopic cycle fluctuation theorem Eq. (7). Thus, the result additionally addresses the conceptual issue of relating entropy production, cycles, and fluctuation theorems that is raised at the end of Ref. [61].

Conceptually, the identification $\mathcal{A} = a(t)$ relies crucially on the observation of transitions rather than states. Two subsequent transitions in the same direction imply a completed cycle with associated entropy production, whereas two visits of the same compound state emerging from state lumping in typical coarse-graining strategies do not. As all transitions except for one are invisible in the present partially accessible system, previous state-based coarse-graining approaches would yield a trivial model containing only a single compound state. Note that alternated observed transitions, observing a forward transition after a backward transition or vice versa, can never imply the completion of an underlying cycle. Therefore, it is not surprising that the estimator of the entropy production of a unicyclic network contains only the statistics of two subsequent transitions in the same direction, as observed in Ref. [61].

IV. MULTICYCLIC NETWORKS WITH ONE OBSERVED TRANSITION

For a general network topology, we cannot reconstruct a unique underlying path contributing to the waiting time distributions $\psi_{I_+ \rightarrow I_+}(t)$ and $\psi_{I_- \rightarrow I_-}(t)$ as in the unicyclic case. Topologically distinct hidden pathways may result in the same pair of consecutive observed transitions. Nevertheless, bounds for the affinities of those cycles that include the observable link can be derived from the ratio $a(t)$. In addition, the cycle lengths of specific cycles can be inferred from the short-time limit of the waiting time distributions. Furthermore, the entropy estimator for unicyclic networks can be generalized to the multicyclic case.

A. Bounds on cycle affinities

For each possible underlying cycle \mathcal{C} with $I_+ \in \mathcal{C}$, Eq. (7) is valid with corresponding cycle affinity $\mathcal{A}_\mathcal{C}$, if $\gamma_{I_+ \rightarrow I_+}^t$ completes the cycle once in the forward direction without taking detours and $\gamma_{I_- \rightarrow I_-}^t$ denotes the corresponding reverse path. Thus, the bound

$$\min_{\mathcal{C}, I_+ \in \mathcal{C}} \mathcal{A}_\mathcal{C} \leq \ln \frac{\mathcal{P}[\gamma_{I_+ \rightarrow I_+}^t | I_+]}{\mathcal{P}[\gamma_{I_- \rightarrow I_-}^t | I_-]} \leq \max_{\mathcal{C}, I_+ \in \mathcal{C}} \mathcal{A}_\mathcal{C} \quad (11)$$

is an immediate consequence for these trajectories $\gamma_{I_+ \rightarrow I_+}^t$ by comparing with the smallest and largest possible affinity, respectively. Remarkably, the inequality in Eq. (7) holds true for general $\gamma_{I_+ \rightarrow I_+}^t$, if the corresponding $\gamma_{I_- \rightarrow I_-}^t$ is defined appropriately by the following algorithm.

- (1) Consider the sequence of states in $\gamma_{I_+ \rightarrow I_+}^t$. For $I_+ = (kl)$, this is $(kl \cdots kl)$.
- (2) Remove the first and last state: $(kl \cdots kl) \mapsto (l \cdots k)$.
- (3) Reading from left to right, remove all closed loops; i.e., as soon as a state m appears twice, remove the intermediate part: $(\cdots amb \cdots cmd \cdots) \mapsto (\cdots amd \cdots)$.
- (4) The remaining *trimmed path* visits each state at most once. This trimmed path completed with I_+ gives rise to a contributing cycle.
- (5) Reverse the trimmed path and reintegrate the first and last state: $(k \cdots l) \mapsto (lk \cdots lk)$.
- (6) Reintegrate the closed loops from step 3 *without* reversing: $(\cdots dma \cdots) \mapsto (\cdots dmb \cdots cma \cdots)$. The resulting sequence of states determines the partial reverse $\mathcal{R}\gamma_{I_+ \rightarrow I_+}^t$, which is of the form $\gamma_{I_- \rightarrow I_-}^t$.

This procedure identifies a trimmed path of $\gamma_{I_+ \rightarrow I_+}^t$ that visits each state at most once. By reversing only this trimmed path, one obtains the partial reverse of $\gamma_{I_+ \rightarrow I_+}^t$, which is denoted by $\mathcal{R}\gamma_{I_+ \rightarrow I_+}^t$. The associated cycle containing the transition I_+ that is reversed by \mathcal{R} has to be one of the possible \mathcal{C} in Eq. (11). For an example of this procedure, see Fig. 2(b). Thus, inverting only the trimmed part of $\gamma_{I_+ \rightarrow I_+}^t$ while maintaining the original direction of the remaining transitions restores the inequality in Eq. (7) and, hence, also the bound in Eq. (11) for every possible microscopic trajectory $\gamma_{I_+ \rightarrow I_+}^t$ with the corresponding partner $\gamma_{I_- \rightarrow I_-}^t = \mathcal{R}\gamma_{I_+ \rightarrow I_+}^t$ defined in this way.

By averaging over all possible trajectory snippets of length t , we can combine Eq. (4) with Eq. (11), which is now valid for all $\gamma_{I_+ \rightarrow I_+}^t$ with corresponding partner $\gamma_{I_- \rightarrow I_-}^t$, to conclude

$$\min_{\mathcal{C}, I_+ \in \mathcal{C}} \mathcal{A}_\mathcal{C} \leq \ln \frac{\psi_{I_+ \rightarrow I_+}(t)}{\psi_{I_- \rightarrow I_-}(t)} \leq \max_{\mathcal{C}, I_+ \in \mathcal{C}} \mathcal{A}_\mathcal{C} \quad (12)$$

for arbitrary $0 < t < \infty$. For this step, it is important to note that the algorithm provides a bijective mapping \mathcal{R} between trajectories of the form $\gamma_{I_+ \rightarrow I_+}^t$ and trajectories of the form $\gamma_{I_- \rightarrow I_-}^t$. The inverse mapping is given by applying the same algorithm to $\gamma_{I_- \rightarrow I_-}^t$ except for reading right to left in step 3 to recover the correct sequence of states for $\gamma_{I_+ \rightarrow I_+}^t$.

The quotient in Eq. (12) can be identified as $a(t)$ via Eq. (5). Thus, the extremal values of $a(t)$ can be identified as bounds on the actual cycle affinity in the form

$$\mathcal{A}_{\mathcal{C}_+} \equiv \max_{\mathcal{C}} \mathcal{A}_\mathcal{C} \geq \sup_{0 \leq t < \infty} a(t) \equiv a_+^*, \quad (13)$$

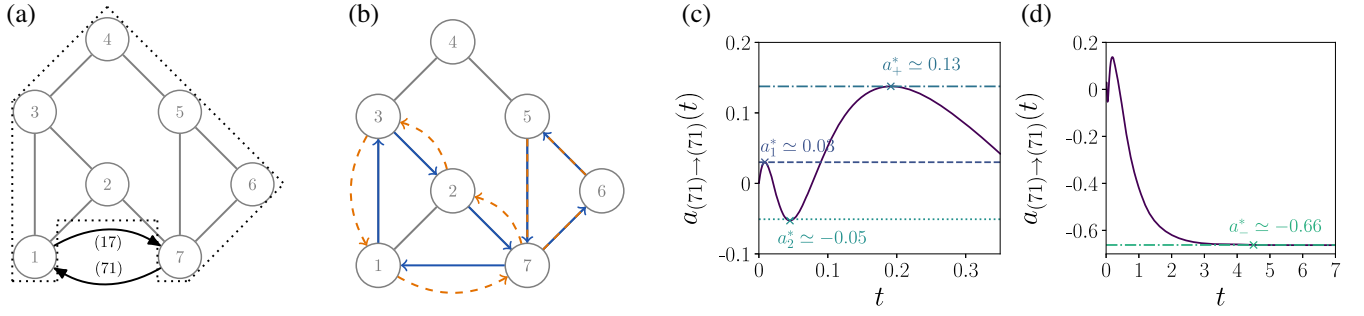


FIG. 2. Illustrative example for a partially accessible multicyclic network. (a) Effective description for a seven-state multicyclic network in which the link between state 1 and state 7 is observable, leading to five different contributing cycles \mathcal{C}_i numbered incrementally. The corresponding transition rates are given in Appendix E. For cycle $\mathcal{C}_0 = (1271)$, the affinity $\mathcal{A}_{\mathcal{C}_0}$ vanishes; the affinity of cycle $\mathcal{C}_1 = (13271)$ is $\mathcal{A}_{\mathcal{C}_1} = 3.18$; the affinity of cycle $\mathcal{C}_2 = (134571)$ is $\mathcal{A}_{\mathcal{C}_2} = -1.43$; the affinity of cycle $\mathcal{C}_3 = (1345671)$ is $\mathcal{A}_{\mathcal{C}_3} = 7.27$; and the affinity of cycle $\mathcal{C}_4 = (1234571)$ is given by $\mathcal{A}_{\mathcal{C}_4} = -5.61$. (b) Example for a trimmed path. For the snippet $\gamma_{I_+ \rightarrow I_+}^t$ depicted with blue arrows, the sequence of visited states is (713276571). The trimmed path for this snippet is (713271) (cf. the algorithm in the main text). The corresponding $\gamma_{I_- \rightarrow I_-}^t$ is not the reversed sequence but rather (176572317) and depicted with dashed orange arrows. Thus, the associated cycle is \mathcal{C}_1 , i.e., $\mathcal{P}[\gamma_{I_+ \rightarrow I_+}^t | I_+] / \mathcal{P}[\gamma_{I_- \rightarrow I_-}^t | I_-] = \mathcal{A}_{\mathcal{C}_1}$. Terms due to the extra loop (7567) cancel in this path weight quotient. (c),(d) Estimation of the cycle affinities of the contributing cycles based on the extreme values of $a_{(71) \rightarrow (71)}(t)$. The maximal value $a_+^* \simeq 0.13$ and the minimal value $a_-^* \simeq -0.66$ of $a_{(71) \rightarrow (71)}(t)$ are lower and upper bounds for the maximal affinity $\mathcal{A}_{\mathcal{C}_3} = 7.27$ and the minimal affinity $\mathcal{A}_{\mathcal{C}_4} = -5.61$, respectively. The initial value $a_{(71) \rightarrow (71)}(0) = a_0^* = 0$ equals the affinity $\mathcal{A}_{\mathcal{C}_0} = 0$ of the shortest network cycle. The local maximum $a_1^* \simeq 0.03$ and the local minimum $a_2^* \simeq -0.05$ can be identified as lower and upper bounds for the affinities $\mathcal{A}_{\mathcal{C}_1} = 3.18$ and $\mathcal{A}_{\mathcal{C}_2} = -1.43$ of the remaining contributing cycles \mathcal{C}_1 and \mathcal{C}_2 , respectively.

$$\mathcal{A}_{\mathcal{C}_-} \equiv \min_{\mathcal{C}} \mathcal{A}_{\mathcal{C}} \leq \inf_{0 \leq t < \infty} a(t) \equiv a_-^*. \quad (14)$$

Here, the maximum and minimum of the affinities are taken over all cycles \mathcal{C} contributing to the observed link. Strong driving along or against the observed link manifests itself in a high positive or negative affinity for a given cycle, respectively. The inequalities (13) and (14) allow us to infer such a source of strong driving from its impact on $a(t)$ from the viewpoint of the observed link. The derived bounds for the cycle affinities are illustrated in Fig. 2. Figures 2(c) and 2(d) show that the extremal affinities $\mathcal{A}_{\mathcal{C}_+}$ and $\mathcal{A}_{\mathcal{C}_-}$ of the contributing cycles are indeed bounded by the maximum value a_+^* and the minimum value a_-^* of $a(t)$. Furthermore, the affinity $\mathcal{A}_{\mathcal{C}_0}$ of the shortest contributing cycle is always equal to the initial value $a_0^* \equiv a(t=0)$ as we prove in the following section.

To quantify the quality of the bounds in Eqs. (13) and (14) for the network from Fig. 2(a), we distinguish two different cases of network realizations. A network with a particular configuration of transition rates belongs to class I if the initial value a_0^* of $a(t)$ is a global maximum or minimum. An exemplary $a(t)$ of a realization of the network belonging to this class is shown in Fig. 3(a), case (I). For this class of network realizations, Eqs. (13) and (14) provide only a single bound for either the maximal or the minimal affinity of the cycles contributing to the observed link. The other bound is satisfied by the shortest cycle with affinity $a_0^* = \mathcal{A}_{\mathcal{C}_0}$. Class II contains the remaining realizations of the network in which $a_0^* = a(t=0)$ is not the

global maximum or minimum. An example for an $a(t)$ sorted into class II is given in Fig. 3(a), case (II); another one is already shown in Figs. 2(c) and 2(d). For this class of network realizations, Eqs. (13) and (14) provide bounds for both the maximal and the minimal affinity of the cycles contributing to the observed link, respectively.

For both classes of rate configurations, quality factors \mathcal{Q} can be defined such that for $\mathcal{Q} = 1$ equality in Eqs. (13) and (14) holds and the value of the bounds equals the actual affinity of the cycle. For $\mathcal{Q} < 1$, the quality factor quantifies the ratio between the value of the bounds and the actual affinity of the corresponding cycle. Using the affinity $\mathcal{A}_{\mathcal{C}_0}$ of the shortest cycle given by a_0^* as a baseline, we introduce the relative distance

$$\Delta a(t) \equiv |a(t) - \mathcal{A}_{\mathcal{C}_0}| = |a(t) - a_0^*|. \quad (15)$$

The quality factors are defined by comparing the maximal value

$$\Delta a_+ = |a_+^* - \mathcal{A}_{\mathcal{C}_0}| \quad (16)$$

and the minimal value

$$\Delta a_- = |a_-^* - \mathcal{A}_{\mathcal{C}_0}| \quad (17)$$

of Eq. (15) with the respective actual distance between the true cycle affinities given by $|\mathcal{A}_{\mathcal{C}_{\pm}} - \mathcal{A}_{\mathcal{C}_0}|$.

For network realizations belonging to class I, either Eq. (13) or Eq. (14) is a bound for the affinity of a single

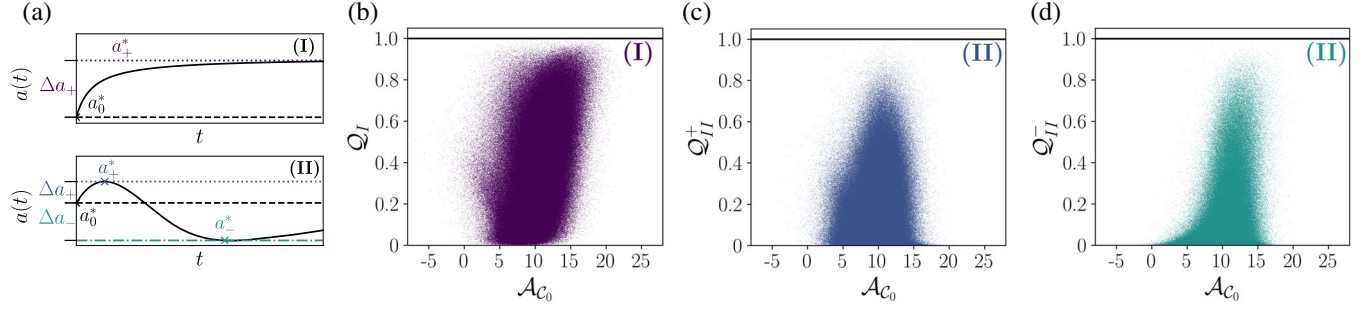


FIG. 3. Quality of the affinity bounds for the seven-state multicyclic network from Fig. 2. (a) Illustration of the quantities entering the definition of the quality factors for the two classes of network realizations. (I) shows $a(t)$ for a network realization belonging to class I. Since a_0^* is the global minimum of $a(t)$, the quality factor \mathcal{Q}_I for this realization is defined according to Eq. (18) with $\Delta a_+ = |a_+^* - a_0^*|$ from Eq. (16). (II) shows $a(t)$ for a network realization belonging to class II. The quality factors \mathcal{Q}_{II}^+ and \mathcal{Q}_{II}^- for this realization are defined according to Eqs. (20) and (21) with $\Delta a_+ = |a_+^* - a_0^*|$ and $\Delta a_- = |a_-^* - a_0^*|$ from Eqs. (16) and (17), respectively. (b)–(d) Quality factors \mathcal{Q}_I , \mathcal{Q}_{II}^+ , and \mathcal{Q}_{II}^- for 2 063 495 randomly drawn rate configurations of the multicyclic network as a function of the affinity \mathcal{A}_{c_0} of the smallest contributing cycle. The mean value of the quality factors \mathcal{Q}_I in (b) is given by $\mathcal{Q}_I \simeq 0.4$, whereas the mean values of the quality factors \mathcal{Q}_{II}^+ in (c) and \mathcal{Q}_{II}^- in (d) are given by $\mathcal{Q}_{II}^+ \simeq 0.2$ and $\mathcal{Q}_{II}^- \simeq 0.1$, respectively. The difference between the quality factors in (c) and (d) for the same class of network realizations is caused by the ensemble for the transition rates that is biased towards positive affinities, explained in detail in Appendix E. All quality factors are determined from the corresponding waiting time distributions derived with the method explained in Appendix A 3.

cycle. If the initial value a_0^* is a global minimum, the maximal affinity \mathcal{A}_{c_+} of the cycles contributing to the observed link is bounded by Eq. (13). Thus, the quality factor \mathcal{Q}_I for this network realization is defined as

$$\mathcal{Q}_I \equiv \frac{\Delta a_+}{|\mathcal{A}_{c_+} - \mathcal{A}_{c_0}|}. \quad (18)$$

If the initial value a_0^* is a global maximum, the minimal affinity \mathcal{A}_{c_-} of the cycles contributing to the observed link is bounded by Eq. (14), and the quality factor \mathcal{Q}_I for this network realization is given by

$$\mathcal{Q}_I \equiv \frac{\Delta a_-}{|\mathcal{A}_{c_-} - \mathcal{A}_{c_0}|}. \quad (19)$$

A graphical illustration of the quantities entering the definition of \mathcal{Q}_I is shown in Fig. 3(a), case (I).

For network configurations belonging to class II, both Eqs. (13) and (14) provide nontrivial bounds for the extremal affinities of the contributing cycles. To distinguish both bounds, two quality factors \mathcal{Q}_{II}^+ and \mathcal{Q}_{II}^- defined similarly to Eqs. (18) and (19) are needed. The quality factor \mathcal{Q}_{II}^+ defined as

$$\mathcal{Q}_{II}^+ \equiv \frac{\Delta a_+}{|\mathcal{A}_{c_+} - \mathcal{A}_{c_0}|} \quad (20)$$

quantifies the quality of the bound Eq. (13) for the maximal affinity \mathcal{A}_{c_+} of the contributing cycles. The quality of the bound Eq. (14) for the minimal affinity \mathcal{A}_{c_-} of the contributing cycles is quantified analogously by

$$\mathcal{Q}_{II}^- \equiv \frac{\Delta a_-}{|\mathcal{A}_{c_-} - \mathcal{A}_{c_0}|}. \quad (21)$$

The quantities entering the definition of \mathcal{Q}_{II}^+ and \mathcal{Q}_{II}^- are illustrated in Fig. 3(a), case (II).

The quality factors for a total of 2 063 495 randomly drawn realizations of the multicyclic network from Fig. 2 are shown in Figs. 3(b)–3(d) as a function of the affinity \mathcal{A}_{c_0} of the smallest contributing cycle. The different structure and mean value of quality factors \mathcal{Q}_I for network realizations from class I, shown in Fig. 3(b), when contrasted to the structures and mean values of quality factors for network realizations from class II, shown in Figs. 3(c) and 3(d), indicate that the partition into two different classes of network realizations corresponds to distinct features of the network that are reflected in these affinity bounds. The mean value of the quality factors for network realizations belonging to class I is given by $\mathcal{Q}_I \simeq 0.4$, which means that the maximal or minimal affinity of the contributing cycles can be estimated based on Eq. (13) or Eq. (14) with an average accuracy of 0.4. This result is remarkable, because, on the one hand, the estimation is based on a noninvasive observation of a single link of the network only and, on the other hand, to our knowledge, no coarse-graining inference scheme exists that bounds affinities of a partially accessible network to this degree of precision. The mean values of the quality factors for network realizations belonging to class II are given by $\mathcal{Q}_{II}^+ \simeq 0.2$ and $\mathcal{Q}_{II}^- \simeq 0.1$, respectively. Compared to the bounds for realizations belonging to class I, realizations belonging to class II tend to quantitatively weaker bounds. However, local maxima and minima of $a(t)$ seem to provide further, loose bounds for the affinities of other,

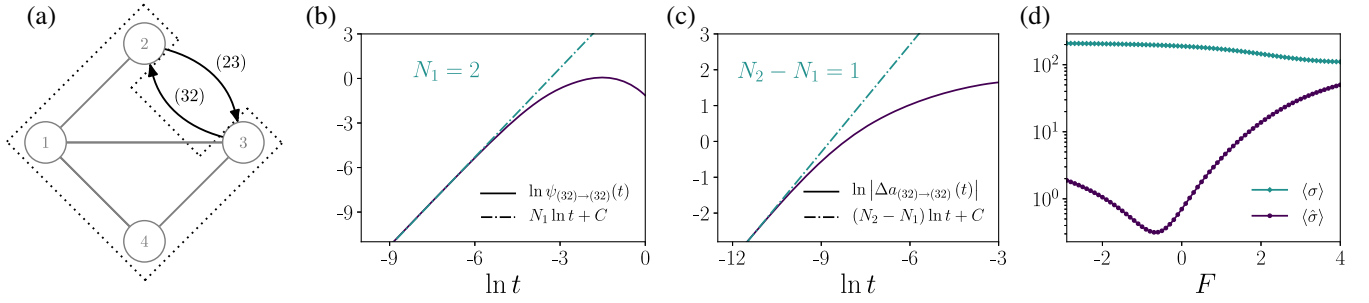


FIG. 4. Inference of cycle lengths and entropy estimation for a partially accessible two-cycle network. (a) Effective description of a four-state network with two cycles in which transitions along the link between states 2 and 3, i.e., (23) and (32), are observable. F is a dimensionless force applied to the observable link between states 2 and 3; all transition rates of the network are given in Appendix E. (b) Inference of the number of hidden transitions N_1 of the smallest network cycle \mathcal{C}_0 based on waiting time distributions calculated with the method from Appendix A 3 for fixed $F = \ln 3$. $N_1 = 2$ corresponds to the slope of the short-time limit of $\ln \psi(t)$ resulting in $|\mathcal{C}_0| = 3$. (c) Inference of the number of hidden transitions N_2 of the second-smallest network cycle \mathcal{C}_1 based on waiting time distributions calculated with the method from Appendix A 3 for fixed $F = \ln 3$. $N_2 - N_1 = 1$ corresponds to the slope of the short-time limit of $\ln |\Delta a(t)|$ resulting in $N_2 = 3$ and $|\mathcal{C}_1| = 4$. (d) The estimator $\langle \hat{\sigma} \rangle$ from Eq. (28) for the mean entropy production $\langle \sigma \rangle$ of the full network as a function of F . The details for the simulations of $\nu_{++}(t)$ and $\nu_{--}(t)$ are given in Appendix E. The method from Appendix A 3 is used to calculate $a(t)$.

nonextremal cycles contributing to the observed link. This numerical finding, illustrated for a given network realization in Fig. 2(c), indicates that each successive maximal and minimal value of $a(t)$ corresponds to a contributing cycle. Therefore, the number of successive maximal and minimal values of $a(t)$ can be interpreted as a lower bound for the total number of contributing cycles for networks from class II.

B. Short-time limit and inference of cycle lengths

Additional information about the network can be obtained from the time dependence of the waiting time distributions $\psi_{I_+ \rightarrow I_+}(t)$ and $\psi_{I_- \rightarrow I_-}(t)$. In the limit $t \rightarrow 0$, only the shortest cycle(s) including the link with forward transition I_+ and backward transition I_- contribute(s) to the waiting time distribution, as longer paths lead to effects of higher order in t . Thus, we can extract the number of hidden transitions N_1 needed to complete the smallest cycle and, if unique, its corresponding affinity $\mathcal{A}_{\mathcal{C}_0}$ from the waiting time distributions via

$$\lim_{t \rightarrow 0} \left(t \frac{d}{dt} \ln \psi_{I_{\pm} \rightarrow I_{\pm}}(t) \right) = N_1 \quad (22)$$

and

$$\lim_{t \rightarrow 0} a_{I_+ \rightarrow I_+}(t) = -\lim_{t \rightarrow 0} a_{I_- \rightarrow I_-}(t) = \mathcal{A}_{\mathcal{C}_0}, \quad (23)$$

respectively, as proven in Appendix C 1. Note that $N_1 + 1$ is equal to the length of the smallest cycle, because, after N_1 hidden transitions, an additional observed transition is needed to complete the full cycle. As an illustration for the identification of N_1 , we consider the ratio of waiting time distributions for the observable link of the two-cycle

network shown in Fig. 4(a). Figure 4(b) illustrates that the evaluation of Eq. (22) for $I_+ = (32)$ coincides with $N_1 = 2$, the minimal number of hidden transitions needed to observe (32) after (32) in the smallest cycle of the network. For the multicyclic network in Fig. 2, the identification of the affinity in Eq. (23) is illustrated in Fig. 2(c) together with the previously discussed affinity bounds, as the affinity $\mathcal{A}_{\mathcal{C}_0}$ of the shortest cycle is reflected in the initial value $a_{(71) \rightarrow (71)}(0) = 0$.

Terms of higher order around $t = 0$ of the form t^N encode similar information about cycles with increasing size contributing to the observable link. Qualitatively, we can extract information about the number of hidden transitions N_2 needed to complete the second-shortest cycle from $a(t)$, since

$$a(t) - a(0) \sim t^{N_2 - N_1}. \quad (24)$$

More quantitatively and as proven in Appendix C 2, the absolute value of the relative distance introduced in Eq. (15) can be seen as the lowest-order perturbation to the shortest cycle. Typically, e.g., if the affinities of the two shortest cycles do not coincide, this effect is due to the second-shortest cycle. In this case, N_2 can be extracted from Eq. (15) via

$$\lim_{t \rightarrow 0} \left(t \frac{d}{dt} \ln |\Delta a_{I \rightarrow J}(t)| \right) = N_2 - N_1 \quad (25)$$

if $N_2 > N_1$, i.e., if the shortest cycle is unique. By combining the results from Eqs. (22) and (25), we can infer N_2 from observable waiting time distributions. Similar to the length of the shortest network cycle, the length of the second-shortest network cycle is given by $N_2 + 1$.

Figure 4(c) illustrates the evaluation of Eq. (25) for $a(t)$ for $I_+ = (32)$ leading to $N_2 - N_1 = 1$. This result is consistent with $N_2 = 3$, the number of hidden transitions needed to observe (32) as the next observable transition after (32) along the second-smallest cycle of the network.

C. Entropy estimator

1. Definition

A time-dependent $a(t)$ implies the presence of a second cycle, as longer waiting times between subsequent transitions hint at the completion of longer pathways. Exploiting this time dependence leads to an entropy estimator that generalizes the estimator of the unicyclic case. To quantify this notion, we let T be the length of a long trajectory with $N + 1$ transitions I_k located at T_{k-1} . The observation starts with the transition I_1 at $T_0 = 0$ and ends with I_{N+1} at time $T_N = T$. Then, the number of subsequent forward or backward transitions with waiting time t in between is given by the time-resolved conditional jump counters defined as

$$\nu_{+|+}(t) \equiv \frac{1}{T} \sum_{m=1}^N \delta(T_m - T_{m-1} - t) \delta_{I_{m+1}, I_+} \delta_{I_m, I_+}, \quad (26)$$

with $\nu_{-|-}(t)$ defined accordingly. These time-resolved conditional jump counters are used together with the ratio of waiting times $a(t)$ defined in Eq. (5) to define a trajectory-dependent entropy estimator

$$\hat{\sigma} \equiv \int_0^\infty dt a(t) [\nu_{+|+}(t) - \nu_{-|-}(t)]. \quad (27)$$

Operationally, $\nu_{+|+}(t)$ and $\nu_{-|-}(t)$ can be obtained from counting conditional transitions up to time t . $a(t)$ can be obtained from histograms for the waiting time distributions based on waiting times between observed transitions. As proven in Appendix B in the limit of long trajectories, i.e., observation times $T \rightarrow \infty$, Eq. (27) defines an entropy estimator respecting time-reversal symmetry in thermodynamic equilibrium whose mean additionally satisfies

$$\langle \hat{\sigma} \rangle \leq \langle \sigma \rangle. \quad (28)$$

This property can be deduced from a fluctuation theorem

$$\hat{\sigma} = \lim_{T \rightarrow \infty} \frac{1}{T} \ln \frac{\mathcal{P}(\Gamma)}{\mathcal{P}(\tilde{\Gamma})} \quad (29)$$

for the trajectory Γ and its time reverse $\tilde{\Gamma}$, both emerging from trajectories of the underlying network by a mapping defined by the effective description of the system. An interpretation for Γ from a mathematical point of view is given in Sec. VI.

2. Illustration and comparison to existing methods

A numerical illustration of the estimator [Eq. (27)] applied to the partially accessible two-cycle network is depicted in Fig. 4(d). The mean entropy production $\langle \sigma \rangle$ and the entropy estimator $\langle \hat{\sigma} \rangle$ are simulated for long, stationary trajectories and different values of a parameter F , which can be interpreted as a driving force applied to the observed link between the states 2 and 3. An external observer who is able to tune the force parameter F can find a value for which the net stationary current $0 = j = \int_0^\infty dt (\nu_{+|+}(t) - \nu_{-|-}(t))$ vanishes. This setup and the particular value of F are referred to as stalling conditions and the stalling force, respectively [39,44,45]. Knowing this stalling force through either measurement or calculation amounts to knowing the effective ‘‘pressure’’ the remaining network exerts on the link (23) against the force F . This information is incorporated in the so-called ‘‘informed partial’’ entropy estimator $\langle \sigma_{\text{IP}} \rangle$ introduced in Ref. [44]. Since the remaining network is taken into account through the effective pressure, $\langle \sigma_{\text{IP}} \rangle$ surpasses the estimator obtained by merely measuring the ‘‘passive partial’’ entropy production $\langle \sigma_{\text{PP}} \rangle$ that can be attributed to the transitions in an observed subset [43], i.e.,

$$\langle \sigma_{\text{PP}} \rangle \leq \langle \sigma_{\text{IP}} \rangle \leq \langle \sigma \rangle \quad (30)$$

as proven in the context of the informed partial estimator in Ref. [45].

Under stalling conditions, both estimators $\langle \sigma_{\text{PP}} \rangle$ and $\langle \sigma_{\text{IP}} \rangle$ become trivial, because they cannot rule out the possibility that the underlying system is at equilibrium if $j = 0$. The introduced time-resolved estimator $\langle \hat{\sigma} \rangle$, however, is able to infer nonequilibrium, since $\langle \hat{\sigma} \rangle > 0$ even if $j = 0$, as additional information enters its definition in Eq. (27). Intuitively, the waiting time distributions encode information about the hidden cycle in their time dependence through a nonconstant $a(t)$. More quantitatively, the estimator $\langle \hat{\sigma} \rangle$ defined by Eq. (27) numerically reproduces the bound of the waiting time distribution based estimator proposed in Ref. [39] for the network in Fig. 4. Both the estimator in Ref. [39] and $\langle \hat{\sigma} \rangle$ share the features of considering successive transitions and adding a time resolution through waiting time distributions. However, $\langle \hat{\sigma} \rangle$ is formulated without the framework of a higher-order semi-Markov process or a Markov chain decimation scheme. While these differences render a general quantitative comparison with our estimator difficult, $\langle \hat{\sigma} \rangle$ beats the informed partial estimator $\langle \sigma_{\text{IP}} \rangle$ for long, stationary trajectories,

$$\langle \sigma_{\text{IP}} \rangle \leq \langle \hat{\sigma} \rangle \leq \langle \sigma \rangle, \quad (31)$$

as we prove in Appendix B 4. Note that the expectation values are still taken in the limit of large observation times in which finite-time effects at the initial and final transition can be neglected. It is also evident from the proof that the

equality is achieved in the first relation if and only if $a(t)$ is time independent. Equality in the second relation is achieved if and only if removing the observed edge results in a network in which detailed balance is satisfied. To give a less formal interpretation of Eq. (31), observational access to the waiting time distributions contains more information than operational access to the observed links via the stalling force F . In particular, it is possible to measure F via

$$-F = \ln \frac{P(I_+|I_+)}{P(I_-|I_-)} = \ln \frac{\langle \int_0^\infty dt \nu_{++}(t) \rangle / \langle n_+ \rangle}{\langle \int_0^\infty dt \nu_{--}(t) \rangle / \langle n_- \rangle}, \quad (32)$$

without perturbing the system at all, as we prove in Appendix B 4.

V. MULTIPLE OBSERVED LINKS IN A MULTICYCLIC NETWORK

Access to additional observable transitions provides further information about the underlying network, which allows us to infer topology qualitatively by identifying allowed and forbidden sequences of transitions and quantitatively by sharpening our entropy estimator for multicyclic networks.

A. Entropy estimator

For M observed links, there are $2M$ possible transitions and a $2M \times 2M$ matrix of quotients

$$a_{IJ}(t) \equiv \ln \frac{\psi_{I \rightarrow J}(t)}{\psi_{J \rightarrow \tilde{I}}(t)} \quad (33)$$

with $I, J \in \{I_+^{(1)}, I_-^{(1)}, \dots, I_-^{(M)}\}$. Here, \tilde{I} is defined as the reverse transition $\tilde{I}_\pm^{(m)} \equiv I_\mp^{(m)}$, which yields a skew symmetry $a_{IJ} = -a_{\tilde{J}\tilde{I}}$. Intuitively, the ratio in Eq. (33) encodes the entropy production term of an effective two-step trajectory $\Gamma_{IJ}^t = I \rightarrow J$ of length t . This term is related to the path weights of microscopic trajectory snippets $\gamma_{I \rightarrow J}^t = k \rightarrow l \rightarrow \dots \rightarrow o \rightarrow p$ of the same length t between two observed transitions $I = (kl)$ and $J = (op)$ in the form

$$a_{IJ}(t) = \ln \frac{\mathcal{P}[\Gamma_{IJ}^t|I]}{\mathcal{P}[\Gamma_{\tilde{J}\tilde{I}}^t|\tilde{J}]} = \ln \frac{\sum_{\gamma_{I \rightarrow J}^t} \mathcal{P}[\gamma_{I \rightarrow J}^t|I]}{\sum_{\gamma_{\tilde{J} \rightarrow \tilde{I}}^t} \mathcal{P}[\gamma_{\tilde{J} \rightarrow \tilde{I}}^t|\tilde{J}]} \quad (34)$$

Similar to the unicyclic case in Eq. (5), unobserved degrees of freedom in the microscopic path $\gamma_{I \rightarrow J}^t$ are integrated out by the summation over the path weights. The ratios in Eq. (33) allow us to generalize $\hat{\sigma}$, defined in Eq. (27), to multiple observed transitions. We define the conditional counters as

$$\nu_{J|I}(t) \equiv \frac{1}{T} \sum_{m=1}^N \delta(T_m - T_{m-1} - t) \delta_{I_{m+1}, J} \delta_{I_m, I}, \quad (35)$$

where we adopt the same notation as in Eq. (26); i.e., the m th transition I_m is located at T_{m-1} . The sum over all $a_{IJ}(t)$ in a trajectory constitutes the entropy estimator

$$\hat{\sigma} \equiv \sum_{IJ} \int_0^\infty dt a_{IJ}(t) \nu_{J|I}(t), \quad (36)$$

which reduces to Eq. (27) in the case of a single link, i.e., two possible transitions $I_\pm = \pm$. Thus, registering a jump J after a previous jump I during an observation of a long trajectory increases $\hat{\sigma}$ by $a_{IJ}(t)$, an antisymmetric increment in which inaccessible data beyond the registered observable one are integrated out. The entropy estimator is thermodynamically consistent in the sense of Eq. (28) and satisfies the fluctuation theorem from Eq. (29) in the long-time limit $T \rightarrow \infty$. Moreover, the definition (36) provides the fluctuating counterpart of the entropy estimator for multicyclic networks introduced in Ref. [61], which is given by $\langle \hat{\sigma} \rangle$ in our notation.

B. Network topology

When we consider multiple transitions, their relative position in the network has a crucial impact on the observed data. For a given network, the waiting time distribution $\psi_{I \rightarrow J}(t)$ depends not only on the pair of transitions I, J , but the entire set of observed links. For example, in the effective description of the network in Fig. 4(a), $a_{(23)(23)}(t)$ is time dependent but becomes time independent if, in addition, the transitions (13) and (31) are observed. The reason is that the fluctuation-theorem-like argument for the affinity can be restored, since observing $\psi_{(23) \rightarrow (23)}(t)$ necessarily implies completion of the cycle $\mathcal{C} = (23412)$. Formulated differently, we can retrace the arguments underlying Eq. (11) to deduce an equality

$$\mathcal{A}_{\mathcal{C}} = \ln \frac{\mathcal{P}[\gamma_{(23) \rightarrow (23)}^t|(23)]}{\mathcal{P}[\gamma_{(32) \rightarrow (32)}^t|(32)]}, \quad (37)$$

because the only possible completed cycle is \mathcal{C} . Based on this observation, we can conclude in more general terms that increasing the number of observed links in a network decreases the possible pathways in the remaining, hidden part of the underlying Markov network. This subnetwork, which is obtained by removing all observed links from the Markov network, is denoted a *hidden subnetwork*. While the hidden subnetwork is made up of the same states as the Markov network, it contains fewer links and, therefore, may be disconnected.

We can make a few technical but far-reaching observations, which are here formulated for long, stationary trajectories; i.e., expectation values are taken in the

NESS and in the limit $T \rightarrow \infty$, as before. Let $I = (kl)$ and $J = (op)$ be two arbitrary observed transitions in the network.

- (1) If the hidden subnetwork is topologically trivial, i.e., does not contain any cycles, then $\langle \hat{\sigma} \rangle = \langle \sigma \rangle$. Moreover, all $a_{IJ}(t)$ are time independent.
- (2) A time-dependent $a_{IJ}(t)$ implies the presence of a cycle in the hidden subnetwork. More precisely, if $a_{IJ}(t)$ is nonconstant in time, then there is a cycle with nonvanishing affinity in the hidden subnetwork that connects the Markov states l and o . In particular, $\langle \hat{\sigma} \rangle < \langle \sigma \rangle$.
- (3) If J cannot be an immediate successor of I , i.e., if $\psi_{I \rightarrow J}(t) = 0$, the Markov states l and o are not connected in the hidden subnetwork. In particular, we can leave out at least one observed transition without decreasing $\langle \hat{\sigma} \rangle$.
- (4) The converse of 2 is not true. It is possible that $a_{IJ}(t)$ is constant in time despite a cycle with nontrivial affinity containing both l and o . However, this behavior is not the generic case but rather requires high symmetry. An explicit example containing such an invisible cycle is provided in Appendix E 5.

These four results are based on the microscopic origin of $a_{IJ}(t)$ as a ratio of path weights as indicated in Eq. (34). The crucial argument is an extension of the reasoning used in the unicyclic case to relate ratios of path weights to the cycle affinity \mathcal{A} [cf. Eq. (7)]. We consider two consecutive transitions $I = (kl)$ and $J = (op)$ and two arbitrary paths γ_1 and γ_2 starting and ending in the Markov states l and o , respectively. Their path weights satisfy

$$\ln \frac{\mathcal{P}[\gamma_1|l]}{\mathcal{P}[\tilde{\gamma}_1|o]} - \ln \frac{\mathcal{P}[\gamma_2|l]}{\mathcal{P}[\tilde{\gamma}_2|o]} = \mathcal{A}_{12}, \quad (38)$$

where \mathcal{A}_{12} is the affinity of the closed loop obtained by appending $\tilde{\gamma}_2$ to γ_1 . If the hidden subnetwork does not contain any cycles, $\mathcal{A}_{12} = 0$ follows trivially. Since γ_1 and γ_2 are arbitrary, Eq. (38) implies the existence of a specific number a_{IJ} satisfying

$$\mathcal{P}[\gamma_{I \rightarrow J}^t | I] e^{a_{IJ} t} = \mathcal{P}[\gamma_{\tilde{J} \rightarrow \tilde{I}}^t | \tilde{J}] \quad (39)$$

for paths $\gamma_{I \rightarrow J}^t$ of arbitrary length t with time reverse $\gamma_{\tilde{J} \rightarrow \tilde{I}}^t$. By summing the previous equation over all possible trajectories of the form $\gamma_{I \rightarrow J}^t$, we conclude

$$a_{IJ}(t) = \ln \frac{\sum_{\gamma_{I \rightarrow J}^t} \mathcal{P}[\gamma_{I \rightarrow J}^t | I]}{\sum_{\gamma_{\tilde{J} \rightarrow \tilde{I}}^t} \mathcal{P}[\gamma_{\tilde{J} \rightarrow \tilde{I}}^t | \tilde{J}]} = \ln \frac{\psi_{I \rightarrow J}(t)}{\psi_{\tilde{J} \rightarrow \tilde{I}}(t)}. \quad (40)$$

In particular, $a_{IJ}(t)$ is time independent if the hidden subnetwork does not contain any cycles or if it satisfies detailed balance; i.e., any cycles in the hidden subnetwork have vanishing affinity. This argument establishes rule 1. To emphasize the relation to our previous results, we note

that Eq. (40) can be seen as a special case of the affinity bounds from Eq. (11), which collapse to equalities if the set of possible \mathcal{A}_C contains only one element. If the hidden subnetwork is a spanning tree, the diagonal element $a_{II} = \mathcal{A}_C$ is the affinity of the cycle C in the unicyclic network obtained by adding the link I back to the hidden subnetwork. In particular, every cycle passes through at least one observed link and is, therefore, registered. Since NESS entropy production stems from cycle currents, it seems plausible to conjecture $\langle \hat{\sigma} \rangle = \langle \sigma \rangle$. Up to contributions from the first and last transition of the trajectory, the statement even holds on the level of individual trajectories in the form

$$\hat{\sigma} = \sigma, \quad (41)$$

as is proven in Appendix D.

Rule 2 is obtained from Eq. (38) by reversing the argument above. Since a nontrivial time dependence $a_{IJ}(t)$ is impossible if \mathcal{A}_{12} vanishes for all γ_1 and γ_2 , there must be at least one cycle with nonvanishing affinity. We now argue that, despite the counterexample given in Appendix E 5, the converse of rule 2 is usually satisfied in a generic setup. If $a_{IJ}(t)$ is constant in time, it equals its limit $a_{IJ}(0)$ as $t \rightarrow 0$. By a timescale separation argument similar to Eq. (23), only the shortest connection between the corresponding Markov states l and o contributes in the short-time limit, whereas longer connections are suppressed and lead to higher-order effects. A hidden cycle containing l and o can be split along these states, giving rise to two topologically distinct pathways γ_1 and γ_2 . Unless both pathways contain the exact same number of states, one class of paths is suppressed by the other in the short-time limit. Thus, the hidden cycle must contain an even number of states to avoid this timescale separation argument. In addition to this purely qualitative argument, generic choices of transition rates generally lead to different first-passage times from l to o depending on the topology of the path, which would also lead to a nontrivial time dependence in $a_{IJ}(t)$.

While the derivation of rule 3 is straightforward from a mathematical point of view, it is of high value operationally, as it can be used to infer the connected components of the hidden subnetwork. In addition, this rule describes a scheme to identify the transitions needed to recover the full entropy production. While rule 2 gives a simple criterion when a particular set of observed transitions is insufficient to conclude $\langle \sigma \rangle = \langle \hat{\sigma} \rangle$, rule 3 formulates a complementary criterion about transitions which are redundant for the entropy estimate. On the level of the Markov network, restoring the minimal number n of observed links I_1, \dots, I_n to connect l and o does not create any cycles in the hidden subnetwork. Since entropy production in the steady state is always due to cycle currents, the entropy production in the hidden subnetwork is not increased by not observing I_1, \dots, I_n , i.e., by adding I_1, \dots, I_n to the hidden subnetwork.

The interplay of statement 2 working "bottom up" and statement 3 coming "top down" is not limited to assessing the quality of the discussed estimator $\hat{\sigma}$. It is also an algorithm for inferring topological aspects of the Markov network by identifying underlying spanning trees, connected components, the position of hidden cycles, and, lastly, their affinities and lengths by combining these rules with the methods introduced in Sec. IV.

VI. UNIFYING SEMI-MARKOV PERSPECTIVE

A. Identification of the semi-Markov description

In the transition-based description, each trajectory ζ of the underlying Markov network is mapped to a trajectory Γ that includes only the observable transitions and the waiting times in between, i.e., symbolically

$$\zeta \mapsto \Gamma[\zeta]. \quad (42)$$

Clearly, this mapping from ζ to Γ is well defined and many-to-one. Adopting a different yet equivalent perspective, this kind of mapping for the underlying trajectory can be seen as a type of milestone using the space of observable transitions for partitioning. Milestoning is a particular coarse-graining scheme from molecular dynamics simulations [68] introduced to stochastic thermodynamics in Refs. [59,60]. In short, the milestones represent certain events, whose occurrence indicates the crossing of a milestone that updates the coarse-grained state of the system.

In practice, this approach results in a semi-Markov description for the coarse-grained system defined on the space of observable transitions. In other words, each observed transition I is identified as a state in the semi-Markov model. The following discussion includes the key concepts of semi-Markov processes in the context of stochastic thermodynamics; see Refs. [56,58,69] for details. The equivalence of the transition-based description to a semi-Markov model becomes evident on the level of single trajectories emerging from the mapping in Eq. (42). An effective trajectory Γ containing $N + 1$ transitions starting and ending with registered transitions I_1 at time $T_0 = 0$ and I_{N+1} at time $T_N = T$, respectively, is fully characterized by the sequence

$$\Gamma = \{(I_1, T_1), (I_2, T_2), \dots, (I_N, T_N)\} \quad (43)$$

for $0 \leq t < T_N$. From a mathematical point of view, the sequence in Eq. (43) precisely defines a particular realization of a semi-Markov trajectory [56], in which the $\{I_k\}$ take the role of the states. Compared to a Markov process, in which the system is fully described by specifying the state i , a full semi-Markov description of the system requires knowing the state I and the waiting time t that has elapsed since I has been entered.

B. Semi-Markov kernels and embedded Markov chain

Since the theory of semi-Markov processes provides the mathematical framework of the effective description, quantities defined for the latter can be expressed in the language of corresponding semi-Markov processes. The waiting time distribution $\psi_{I \rightarrow J}(t)$ assigned to each transition I , dubbed as intertransition time density in Ref. [61], is called the semi-Markov kernel in this framework. A semi-Markov kernel $\psi_{I \rightarrow J}(t)$ is defined as the joint distribution of waiting time t and transition destination J if the actual state is I with age zero, which coincides precisely with the definition of the waiting time distributions in Eq. (3). Integrating out the waiting time t of a semi-Markov kernel results in conditional probabilities

$$p_{IJ} \equiv P(J|I) = \int_0^\infty dt \psi_{I \rightarrow J}(t) \quad (44)$$

for a transition between two semi-Markov states irrespective of the waiting time in I . These probabilities, whose ratios are already used in Eq. (9), can now be placed in a mathematical context. Based on the transition probabilities p_{IJ} defined by Eq. (44), the concept of the embedded Markov chain (EMC) can be established for every semi-Markov process by integrating out its time variable [56]. The embedded Markov chain of the effective trajectory in Eq. (43) is given by the sequence

$$\Gamma_{\text{EMC}} = (I_1, I_2, \dots, I_{N+1}) \quad (45)$$

of observed transitions. The transition probabilities of the corresponding discrete-time Markov process are given by Eq. (44).

C. Path weight and time-reversal operation

According to the semi-Markov description, the path weight $\mathcal{P}[\Gamma|I_1, 0]$ of the effective trajectory $\Gamma(t)$ conditioned on the first transition is simply given by

$$\mathcal{P}[\Gamma|I_1, 0] = \prod_{i=1}^N \psi_{I_i \rightarrow I_{i+1}}(t_i), \quad (46)$$

with $t_i = T_i - T_{i-1}$, where we follow the conventional definition [56,69–71]. Equation (46) coincides with the effective path weight defined for trajectories of the transition-based description in Ref. [61]. Note that the first and last transitions do not need to be treated differently [56,58,69,72], since the trajectory starts and ends with a transition by construction.

The time-reversal operation for the present semi-Markov process is not given by the conventional time-reversal operation for semi-Markov processes. Instead of simply reversing Γ in time, as proposed in Refs. [56,70], two peculiarities emerging from the time reversal of the

underlying trajectory ζ have to be taken into account. First, Γ contains observed transitions that are odd under time reversal similar to momenta and, therefore, need to be reversed [39,59,73]. Thus, it is natural to define the reversed transition \tilde{I} for a transition I as

$$I = (kl) \rightarrow \tilde{I} \equiv (lk). \quad (47)$$

Second, we observe an effect introduced as *kinetic hysteresis* in Ref. [59]. After registering a transition $I = (ij)$ at time t_I , it would be misleading to treat I as a compound state and conclude that the underlying system remains in I until the next transition J is observed at t_J . At some time t with $t_I \leq t \leq t_J$, the state of the coarse-grained system is described completely by knowing the last transition I and the time $t - t_I$ that has passed since then. However, the same point in time on the reversed trajectory is described by knowing that $t_J - t$ has passed since the last transition \tilde{J} . Thus, \tilde{J} replaces I as the latest registered transition. Combining both effects allows us to formulate the time reversal of a semi-Markov kernel $\psi_{I \rightarrow J}(t_J - t_I)$ as

$$\tilde{\psi}_{I \rightarrow J}(t_J - t_I) \equiv \psi_{\tilde{J} \rightarrow \tilde{I}}(t_J - t_I), \quad (48)$$

resulting in

$$\mathcal{P}[\tilde{\Gamma}|I_N, T] = \prod_{i=1}^{N-1} \psi_{\tilde{I}_i \rightarrow \tilde{I}_{i-1}}(t_i), \quad (49)$$

for the conditioned path weight $\mathcal{P}[\tilde{\Gamma}|I_N, T]$ of the time-reversed trajectory $\tilde{\Gamma}$. Clearly, the time reversal in Eq. (48) is identical to the time reversal proposed in Ref. [61], since the shift of intertransition times discussed there is precisely the effect of kinetic hysteresis described above. Note that the modifications to the time-reversal operation of the semi-Markov process arise naturally, in accordance with the paradigm that time reversal does not commute with coarse-graining of the form Eq. (42), in general [59].

In the common conception of semi-Markov processes, the direction-time independence criterion is a necessary condition to ensure time-reversal symmetry in equilibrium [56,70]. Remarkably, the semi-Markov process as introduced here breaks this condition, in general. This apparent contradiction is resolved, since the derivation of the direction-time independence relies crucially on the conventional time-reversal operation for semi-Markov processes, which does not apply here, as discussed above.

D. Interpretation of the entropy estimators

The entropy estimator $\langle \hat{\sigma} \rangle$ is established for unicyclic networks in Eq. (10). It is based on the microscopic fluctuation theorem in Eq. (8) valid for the ratio of waiting time distributions. The generalization of $\langle \hat{\sigma} \rangle$ for multicyclic networks with multiple observed links in Eq. (36), which

includes the estimator for a single observed link Eq. (27) as a special case, relies on the same fluctuation theorem generalized to the multicyclic case. From the semi-Markov perspective, these fluctuation theorems can be interpreted as the consequence of an actual fluctuation theorem of the semi-Markov process. We define the semi-Markov entropy production rate σ_{SM} as the limit

$$\sigma_{\text{SM}} \equiv \lim_{T \rightarrow \infty} \frac{1}{T} \ln \frac{\mathcal{P}(\Gamma)}{\mathcal{P}(\tilde{\Gamma})}, \quad (50)$$

which differs from the known expressions, e.g., in Refs. [69,72,74] because of the modified time-reversal operation. Comparing Eq. (50) to Eq. (29), we conclude that σ_{SM} , in fact, equals $\hat{\sigma}$, which is established as a thermodynamically consistent coarse-grained entropy production term in the previous sections. In hindsight, the fluctuation theorem in Eq. (8) can be derived from Eq. (50) by specifying to semi-Markov trajectories with only a single transition. The underlying Markov description does not enter explicitly anymore; instead, it is incorporated implicitly by ensuring that σ_{SM} is the correct physical entropy production. The affinity estimators derived in Sec. IV can also be seen as consequences of Eq. (50), tracing back the entropy production to the level of contributing cycles.

From the unifying semi-Markov perspective, we can give three complementary interpretations of the estimator $\langle \hat{\sigma} \rangle$. First, the derivation presented in Ref. [61] relies on the information-theoretical identification of the expected entropy production of a stochastic process as a Kullback-Leibler divergence between the path weights of a forward and backward process [36,37]. Second, contributions to the fluctuating quantity $\hat{\sigma}$ can be attributed to the completion of cycles in the underlying Markov network, which are partially observed for an external observer. Third, $\hat{\sigma} = \sigma_{\text{SM}}$ can be interpreted as the entropy production rate of a semi-Markov process with a particular time-reversal operation. Thermodynamic consistency of $\hat{\sigma}$ is then coupled to the applicability of the time-reversal operation, which has to be established from the underlying network.

By interpreting $\hat{\sigma}$ as the entropy production σ_{SM} of the equivalent semi-Markov process, the decomposition proposed in Ref. [61] can be identified as a decomposition of $\langle \sigma_{\text{SM}} \rangle$ into the entropy production $\langle \sigma_{\text{EMC}} \rangle$ of the EMC and the remaining entropy production $\langle \sigma_{\text{WTD}} \rangle$ caused by the waiting times:

$$\langle \sigma_{\text{SM}} \rangle = \langle \sigma_{\text{EMC}} \rangle + \langle \sigma_{\text{WTD}} \rangle. \quad (51)$$

Up to a time conversion factor, $\langle \sigma_{\text{EMC}} \rangle$ is the mean entropy production of the EMC, which is given by

$$\langle \sigma_{\text{EMC}} \rangle = \frac{1}{\langle t \rangle} \sum_{I,J} p_I^s p_{IJ} \ln \frac{p_{IJ}}{p_{JI}}, \quad (52)$$

where p_I^s is the steady state of the EMC as a discrete-time Markov chain. The factor $\langle t \rangle$, the average waiting time between two transitions, is needed because entropy production of a discrete-time Markov chain is naturally measured per step rather than per time. In terms of the application to observed links, p_I^s quantifies the relative frequency of a particular transition I in a long sequence of observed transitions as given by Eq. (45). Equivalently, Eq. (52) can be derived as the mean of

$$\sigma_{\text{EMC}} \equiv \lim_{T \rightarrow \infty} \frac{1}{T} \ln \frac{\mathcal{P}[\Gamma_{\text{EMC}}]}{\mathcal{P}[\tilde{\Gamma}_{\text{EMC}}]}, \quad (53)$$

defined on the level of single trajectories Γ_{EMC} based on the arguments presented in Appendix B 3. Note that Eq. (52) coincides with Eq. (49) in Ref. [61], dubbed there as transition sequence contribution to the entropy estimator. Since the EMC emerges from integrating out the temporal resolution of the semi-Markov process, $\langle \sigma_{\text{EMC}} \rangle$ vanishes in situations with no observable net current. In other words, the contribution of a particular pair of transitions I, J to σ_{EMC} vanishes if and only if the net number of transitions J after previous I matches the number of transitions \tilde{J} after previous \tilde{I} on average, i.e., if $\mathcal{P}[\Gamma_{\text{EMC}}] = \mathcal{P}[\tilde{\Gamma}_{\text{EMC}}]$.

The condition of vanishing $\langle \sigma_{\text{EMC}} \rangle$ can also be related to the stalling conditions. In fact, the entropy production associated with the embedded Markov chain coincides with the informed partial entropy estimator $\langle \sigma_{\text{IP}} \rangle$ formulated for the case of one accessible transition [44,45], i.e.,

$$\langle \sigma_{\text{IP}} \rangle = \langle \sigma_{\text{EMC}} \rangle, \quad (54)$$

as proven in Appendix B 4. In particular, the force F can be determined as

$$\ln \frac{p_{I_+ I_+}}{p_{I_- I_-}} = \ln \frac{P(I_+ | I_+)}{P(I_- | I_-)} = -F \quad (55)$$

by virtue of Eq. (32) without referring to waiting times at all. This result is not surprising, since both estimators measure the affinity \mathcal{A}_C of a single, averaged ‘‘effective cycle’’ either through the applied force F or through the ratio $\ln P(+|+)/P(-|-)$. Without the time resolution, the estimator $\langle \hat{\sigma} \rangle$ loses the ability to distinguish between longer or shorter hidden cycles. Thus, we can reformulate a conjecture proposed in Ref. [61] that states that $\langle \sigma_{\text{EMC}} \rangle$ exceeds an analogous expression based on the TUR, $\langle \sigma_{\text{TUR}} \rangle$, since $\langle \sigma_{\text{EMC}} \rangle \geq \langle \sigma_{\text{TUR}} \rangle$ is equivalent to $\langle \sigma_{\text{IP}} \rangle \geq \langle \sigma_{\text{TUR}} \rangle$. As another consequence of Eq. (54), the fluctuation theorem proven in Ref. [45] for σ_{IP} , the fluctuating counterpart of the estimator $\langle \sigma_{\text{IP}} \rangle$, is related to its counterpart for the EMC, Eq. (52).

The second expression in Eq. (51), $\langle \sigma_{\text{WTD}} \rangle$, can be deduced by transferring the splitting of the entropy production into contributions from the EMC and remaining contributions from the waiting times to individual

semi-Markov kernels in the path weights. In more practical terms, a single semi-Markov kernel $\psi_{I \rightarrow J}(t)$ can be decomposed into

$$\psi_{I \rightarrow J}(t) = p_{IJ} \cdot \psi(t|IJ), \quad (56)$$

separating the contribution from the EMC from a conditional waiting-time kernel $\psi(t|IJ) = \psi_{I \rightarrow J}(t)/p_{IJ}$. By decomposing all kernels in the path weights using Eq. (56), we can identify $\langle \sigma_{\text{WTD}} \rangle$ as a Kullback-Leibler divergence between the normalized probability densities $\psi(t|IJ)$ and their reverse $\psi(t|\tilde{J}\tilde{I})$. Thus, the derivation in Ref. [61] relates to factorizing out the EMC according to Eq. (56) in the context of semi-Markov processes. Using Eq. (40), we see that $\langle \sigma_{\text{WTD}} \rangle$ vanishes if and only if all $a_{IJ}(t)$ are constant in time. In particular, all $a_{IJ}(t)$ are constant in time if detailed balance is satisfied in the hidden subnetwork.

The decomposition of the semi-Markov entropy production in Eq. (51) clarifies additionally the relation between the estimator $\langle \hat{\sigma} \rangle$ and the entropy estimator $\langle \sigma_{\text{KLD}} \rangle$ introduced in Ref. [39], which is also decomposed in the form

$$\langle \sigma_{\text{KLD}} \rangle = \langle \sigma_{\text{aff}} \rangle + \langle \tilde{\sigma}_{\text{WTD}} \rangle. \quad (57)$$

Similar to Eq. (51), this decomposition into contributions from waiting time distributions and affinities is obtained by splitting off the EMC. The analogy is further strengthened by noting that

$$\langle \sigma_{\text{aff}} \rangle = \langle \sigma_{\text{IP}} \rangle = \langle \sigma_{\text{EMC}} \rangle, \quad (58)$$

with the first equality proven in Ref. [39]. Note that the respective embedded Markov chains are different objects, as $\langle \sigma_{\text{aff}} \rangle$ refers to a coarse-grained unicyclic three-state model, whereas $\langle \sigma_{\text{EMC}} \rangle$ observes only a single transition of this model. Nevertheless, the result is not entirely surprising in hindsight, since $\langle \sigma_{\text{EMC}} \rangle$ recovers the full entropy production of a unicyclic model by virtue of Eq. (9).

The difference between the estimators $\langle \sigma_{\text{WTD}} \rangle$ and $\langle \tilde{\sigma}_{\text{WTD}} \rangle$, or $\langle \hat{\sigma} \rangle$ and $\langle \sigma_{\text{KLD}} \rangle$, respectively, emerges from different rationales underlying the respective semi-Markov processes. Describing a physical system with a semi-Markov process is not sufficient to determine its entropy production uniquely, since the correct time-reversal operation needs to be discussed separately [39,66,67]. In total, three different time-reversal operations for semi-Markov processes are implicitly used to define entropy estimators for partially accessible Markov networks.

- (1) *Conventional time reversal*, $\tilde{\Gamma}(t) = \Gamma(T - t)$.—In this case, physically consistent semi-Markov processes satisfy direction-time independence [70], which causes $\langle \sigma_{\text{WTD}} \rangle$ to vanish [56]. This time-reversal operation is applicable to particular settings

of coarse-graining [56,58]. States do not change, i.e., are even under time reversal.

- (2) *Modified time reversal, introduced above.*—This operation includes the kinetic hysteresis effect introduced [59], which is natural for coarse-graining based on milestoneing [60]. In our case, semi-Markov states model transitions, which are odd under time reversal.
- (3) *Time reversal for second-order semi-Markov processes, introduced in Ref. [39].*—States in a second-order semi-Markov process are doublets containing the previous and current state by construction. Because of this memory effect, states are neither even nor odd under time reversal.

Any of these operations can be used to define an entropy via Eq. (50). This entropy can always be split according to Eq. (56), where the resulting waiting-time contributions are given by 0 , $\langle\sigma_{\text{WTD}}\rangle$, and $\langle\tilde{\sigma}_{\text{WTD}}\rangle$, respectively. In addition, any of the discussed operations are involutions, each giving rise to a dual dynamics for which an appropriate fluctuation theorem holds for the corresponding entropy production [3]. At this level, any nonvanishing entropy production quantifies a different mathematical notion of irreversibility, which becomes a thermodynamic quantity only if the time reversal is known to be justified physically [59].

VII. CONCLUSION

A. Summary and discussion

In this paper, we have introduced an effective description for partially accessible Markov networks based on the observation of transitions along individual links and waiting times between successive observed transitions. The corresponding waiting time distributions yield an entropy estimator $\langle\hat{\sigma}\rangle$. The corresponding fluctuating counterpart $\hat{\sigma}$ additionally obeys a fluctuation theorem and was shown to have a natural interpretation as a semi-Markov entropy production. On a microscopic level, we have discussed with cycle fluctuation theorem arguments why observing one link suffices to recover the full entropy production in a unicyclic network. More generally, we have derived an operational criterion that indicates the absence of hidden cycles, which guarantees $\langle\hat{\sigma}\rangle = \langle\sigma\rangle$.

If the hidden part of the network contains hidden cycles, we have shown that the estimator $\langle\hat{\sigma}\rangle$ yields a lower bound on the entropy production, which has been shown to improve on known estimation methods. Additionally, we have shown that the waiting time distributions contain information about topology and cycle affinities of the hidden network. To extract this information, we have derived exact results and estimation methods, whose quality has been assessed numerically. Both the entropy estimator and the affinity estimators are built upon the generalized microscopic cycle fluctuation theorem argument which is, as we have shown, the signature of a

fluctuation theorem valid for an effective semi-Markov process. From the perspective of this semi-Markov process, we have unified extant entropy estimators by providing a mathematical interpretation.

Different inference methods can be compared based on the required input data and the significance of their predictions. In the case of a single link, $\langle\hat{\sigma}\rangle$ relies on the measurement of statistical data contributing to a single current. While the amount of input data is comparable to methods based on the TUR, the predictions generally are much stronger, at least in the unicyclic case. While the TUR provides lower bounds on entropy production and cycle affinity in this case [23], we recover exact values for both quantities even without access to the waiting times. When the waiting time distributions are available, exact cycle lengths can be deduced, which improves significantly on a known TUR-based trade-off relation between affinity and cycle length [32,33].

In terms of predictive significance, the entropy estimator is comparable to the method introduced in Ref. [39] that is based on knowing a coarse-grained subnetwork, but it requires substantially less information. Calculating $\hat{\sigma}$ is possible without any knowledge about the underlying network beyond a single observed link. In particular, the issue of decimation schemes for coarse-graining is circumvented completely. Rather, the entropy estimator $\hat{\sigma}$ combines current measurements with information-theoretical notions via conditional counting, since our expectation on the next transition depends explicitly on the previous one [36]. Thus, the sequence of transitions forms a Markov chain, which is identified as the EMC in the corresponding semi-Markov description. A mathematical discussion of semi-Markov processes allows us to clarify physically distinct categories of semi-Markov descriptions depending on the correct underlying time-reversal operation. Although different entropylike quantities satisfy fluctuation theorems and provide a mathematical notion of irreversibility, the thermodynamically consistent entropy production must be identified by more fundamental means. If measuring the entropy production is feasible operationally, this knowledge can be used to decide which time-reversal operation recovers the correct entropy production. In this sense, identifying the correct time-reversal operation is a task of thermodynamic inference.

B. Perspectives

The transition-based effective description for partially accessible Markov networks and the derived estimators for entropy and topology open a wide range of possible subsequent research topics. First of all, it will be promising to generalize the estimators for affinity and cycle length to networks with multiple observable links. Based on such a generalization, it would become possible to apply the estimators to a broader range of networks. The combined observation of different links would make it additionally

possible to infer more information about the network, because different affinities and cycle lengths would be accessible.

With the macroscopic limit of large, complex systems in mind, it is an obvious, albeit ambitious, challenge to transfer thermodynamic inference methods to Markov networks whose cycles outnumber the observed links by far. Conceptually, the ratio of waiting time distributions separates the time-resolved notion of irreversibility from other time-dependent effects entering a waiting time distribution. The estimation techniques for topology and affinity that are based on the short-time limit and, hence, short pathways infer local properties of Markov networks that may even be large. Passing from local to global methods would require a different approach. The dominant parts of the large-scale network structure might become manifest in patterns of particular transition sequences or waiting times in long trajectories. Splitting these into smaller snippets as proposed here is a first step toward a future study of self-correlations in a long trajectory to extract more complex structures.

To gain more insight into the effective description from the established perspective of coarse-graining, one should investigate how existing coarse-graining strategies for observable states [43,44,48–55,57] are related to the approach introduced here. By combining these complementary approaches and by taking into account conclusions on milestoneing [59,60], the concept of coarse-graining can potentially be generalized to a more fundamental level. From a practical perspective, we may ask how the method can be generalized to less ideal situations, e.g., if the observer cannot distinguish between different transitions or registers particular patterns or sequences of transitions only. This class of situations also includes the complementary problem when particular states can be observed rather than particular transitions, because observing the arrival in a state is equivalent to observing all transitions into this state without the ability to distinguish between them.

The potential of waiting time distributions and their role for inference schemes is certainly not exhausted by the results presented here. Combining the estimators for entropy production and network topology with existing numerical methods may increase the usefulness of the waiting time distributions in thermodynamic inference schemes. Fitting rates of the underlying Markov network to the recorded waiting time distribution [42] or using minimization methods [40,41] are promising tools to obtain tighter, more specialized bounds for the discussed estimators or even to reconstruct the transition rates in a small network from sufficient data. These methods will gain particular practical relevance, since topological aspects of the underlying network can be deduced rather than have to be assumed.

Furthermore, even though the effective description has been introduced and discussed for observable transitions of a partially accessible Markov network in the NESS, it is, in principle, not limited to this setting. For example, the description could be applied beyond the steady state to analyze transient dynamics. Finally, it would be interesting to apply the approach to a Langevin dynamics to explore the adjustments needed for systems with continuous degrees of freedom.

APPENDIX A: WAITING TIME DISTRIBUTIONS FROM PATH WEIGHTS AND TRAJECTORY SNIPPETS

1. Markovian path weights and master equation

We consider the effective description of a given, only partially accessible system in which transitions are observed, e.g., the effective two-cycle network from the main text based on the observation of transitions between states 2 and 3, shown in Fig. 5. We assume that there is an underlying, more fundamental network to which a discrete Markovian description from the perspective of stochastic

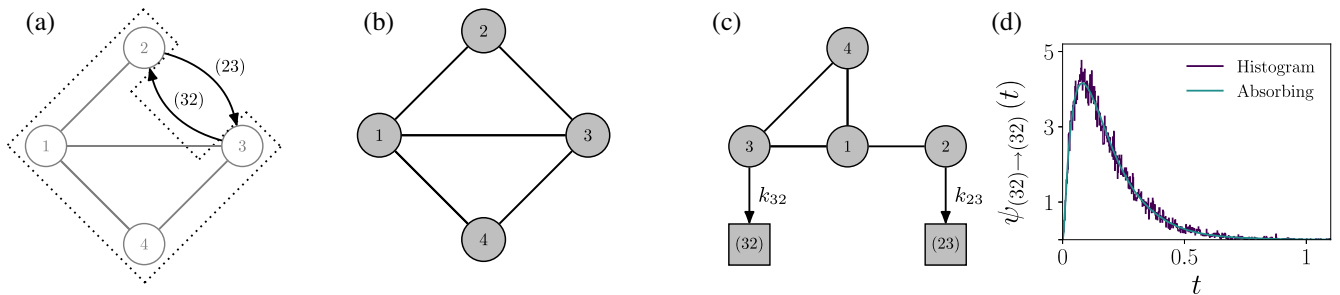


FIG. 5. Example for the analytical calculation of waiting time distributions based on effective absorbing dynamics. (a) Effective description for the partially accessible two-cycle network from the main text. Only transitions from state 2 to state 3 and in the reversed direction are observable. (b) Underlying Markov network. On the fundamental level of description, the network is Markovian, and transitions from state k to state l are governed by the transition rate k_{kl} . (c) Effective absorbing Markov network. Between two observed transitions, the system can be described with an absorbing master equation. This intermediate hidden dynamics is terminated by either a transition (32) or a transition (23). (d) Exemplary waiting time distribution derived from the numerical solution of the absorbing master equation for the effective dynamics and the corresponding distribution determined from a histogram of the waiting times within a trajectory of length $T = 10^7$ generated with a Gillespie simulation [75] of the network. The transition rates of the network are drawn randomly.

thermodynamics, as described in detail in Ref. [3], can be applied. For the effective description in Fig. 5(a), this full Markov network with two fundamental cycles is shown in Fig. 5(b).

Transitions from state k to state l are governed by a transition rate k_{kl} , which is independent of the time already spent in the state k due to the Markov property of the description. Thus, the waiting time distribution in a particular state must be memoryless and, therefore, exponentially distributed. In formulas, the probability density for surviving in state k until exactly time t is given by $\Gamma_k \exp(-\Gamma_k t)$, where $\Gamma_k = \sum_l k_{kl}$ denotes the escape rate of state k . Given that state k is exited, a transition to state l is weighted with the transition rate and, therefore, happens with the transition probability $k_{kl}/\sum_l k_{kl}$.

Based on the discussed survival and transition probabilities, a path weight quantifying the probability of a trajectory ζ of the Markov network can be introduced. We assume that the network has N states, is fully connected and that there are no unidirectional links; i.e., $k_{kl} > 0$ implies $k_{lk} > 0$. The path weight $\mathcal{P}[\zeta(t)]$ for a generic trajectory $\zeta(t)$ conditioned on the initial state k_0 at time $t = 0$ is given by

$$\mathcal{P}[\zeta(t)|k_0, 0] = \prod_{k=1}^N \exp(-\Gamma_k \tau_k) \prod_{(kl)} k_{kl}^{n_{kl}}, \quad (\text{A1})$$

where the second product runs over all possible transitions (kl) in the network. The trajectory-dependent quantities τ_k and n_{kl} denote the total time spent in state k and the total number of transitions (kl) in $\zeta(t)$, respectively.

In principle, a trajectory-dependent observable can be obtained by a path integral over all trajectories ζ , which in practice means summing over the number L of possible jumps and integrating over all transition times t_1, \dots, t_L . An important consequence is that the probability to observe L jumps in a short trajectory ζ of length Δt scales as $P(L \text{ jumps}) \sim \Delta t^L$ for $\Delta t \rightarrow 0$, since

$$P(\zeta \text{ contains exactly } L \text{ jumps} | k_0, 0) = \prod_{l=1}^L \left(\int_0^{\Delta t} dt_l \right) \mathcal{P}[\zeta(t)|k_0, 0] \sim \Delta t^L [1 + \mathcal{O}(\Delta t)], \quad (\text{A2})$$

because the path weight as given in Eq. (A1) is of the order of 1 in Δt . Thus, a first-order differential equation governing the time evolution of $\zeta(t)$ can be derived by calculating the path weights for constant and one-jump trajectories, which are the only terms containing terms of first order in Δt . The resulting differential equation

$$\partial_t p_k(t) = \sum_{l \neq k} [p_l(t)k_{lk} - p_k(t)k_{kl}(t)] \quad (\text{A3})$$

is known as the master equation and can be solved to obtain $p_k(t)$, the probability to find the system in state k at time t . Since the master equation description Eq. (A3) is equivalent to the path weight description, solving the initial value problem for $p_k(0) = \delta_{k_0 k}$ amounts to calculating

$$p_k(t) = P[\zeta(t) = k | \zeta(0) = k_0] \quad (\text{A4})$$

$$= \sum_{\zeta(t)=k} \mathcal{P}[\zeta(t)|k_0, 0]. \quad (\text{A5})$$

The symbolic notation of a sum over paths is used repeatedly in the following calculations.

2. From fully accessible networks to partially accessible networks

On a coarse-grained level of description, the trajectories of the network are only partially accessible. Thus, a complete analytical description by solving the master equation (A3) is generally impossible, because even the underlying fundamental network may be unknown.

In the following, we assume that transitions along a single link connecting the Markov states k and l can be observed but not the states themselves. This transition-based description coincides with the description proposed in Ref. [61]. Adopting the notation from the main text, a transition along this link $k \rightarrow l$ and its reverse $l \rightarrow k$ are abbreviated as $I_+ = (kl)$ and $I_- = (lk)$, respectively. Since the sequence of observed jumps and the waiting times in between are the only accessible information about the system in our effective description, a typical example of an observed effective trajectory Γ may look like

$$\Gamma = ? \rightarrow I_+ \rightarrow I_+ \rightarrow I_- \rightarrow I_+ \rightarrow \dots$$

at jump times $?, T_0, T_1, T_2, T_3, \dots$, (A6)

where $?$ represents the unknown transition of the system in the past prior to the first observed transition.

For simplicity, we assume from now on that the process starts and ends immediately after the observation of an observable transition I_1 at time $T_0 = 0$, I_{N+1} at time $T_N = T$, to address the core of our argumentation without worrying about non-time-extensive initial and final terms of the trajectory. Moreover, the scheme indicated in Eq. (A6) can be generalized to any number of observable links. We write $I_n = (k_n l_n)$ as the n th observed transition between the underlying states k_n and l_n , where we note that $l_n \neq k_{n+1}$, in general, as hidden dynamics cannot be excluded. Schematically, a coarse-grained trajectory Γ takes the form

$$\Gamma = I_1 \rightarrow I_2 \rightarrow I_3 \rightarrow \cdots \rightarrow I_N \rightarrow I_{N+1}$$

at jump times $T_0 = 0, T_1, T_2, \dots, T_{N-1}, T_N = T$. (A7)

Similar to the Markov case, the probability for Γ can, in principle, be quantified by a path weight description. First of all, it is important to note that no memory effects ranging over multiple observed transitions need to be considered. The path weight for the future of the trajectory, i.e., the path weight for the trajectory after a transition I_n is registered, is unaffected by the previous block $I_{n-1} \rightarrow I_n$, since knowing the transition $I_n = (k_n I_n)$ at t_n implies knowing the state of the underlying Markovian system immediately after T_{n-1} . Thus, the path weight can be split into parts belonging to observed transitions:

$$\mathcal{P}[\Gamma(t)|I_1, 0] = P(I_2, T_1|I_1, 0)P(I_3, T_2|I_2, T_1) \cdots P(I_{N+1}, T_N|I_N, T_{N-1}), \quad (\text{A8})$$

with $P(J, T_J|I, T_I)$ denoting the probability for observing transition J at time T_J if transition I is observed at time T_I .

Constituting the elementary building blocks in the coarse-grained picture, the objects $P(J, T_J|I, T_I)$ quantify the probability for observing J after a given I with waiting time $T_J - T_I$ in between. Thus, Eq. (A8) can also be written as

$$\mathcal{P}[\Gamma(t)|I_1, 0] = \psi_{I_1 \rightarrow I_2}(t_1) \psi_{I_2 \rightarrow I_3}(t_2) \cdots \psi_{I_N \rightarrow I_{N+1}}(t_N), \quad (\text{A9})$$

with $t_i = T_i - T_{i-1}$ and $t_1 = T_1$ in terms of the waiting time distribution

$$\psi_{I \rightarrow J}(t) = P(J, t|I, 0), \quad (\text{A10})$$

according to the definition of $\psi_{I \rightarrow J}(t)$ in Eq. (3). The waiting time distributions are normalized in the form

$$\sum_J \int_0^\infty dt \psi_{I \rightarrow J}(t) = 1, \quad (\text{A11})$$

whereas integrating out the time variable gives the marginal distribution

$$p_{IJ} \equiv \int_0^\infty dt \psi_{I \rightarrow J}(t) = P(\text{next observed transition is } J | \text{last observed transition is } I). \quad (\text{A12})$$

3. Effective absorbing dynamics

On a fundamental level, we are interested in how the path weights of the effective description Eq. (A9) and their elementary building blocks Eq. (A10) are linked to the path weights Eq. (A1) of the corresponding microscopic trajectories of the full network. As a first step, we note that the way in which the effective trajectory Γ is split carries over to a splitting on the fundamental level for the microscopic trajectory ζ , because not only the coarse-grained but the entire microscopic state is known at the observed transition events. Symbolically, this can be denoted as

$$\zeta \hat{=} \gamma_{I_1 \rightarrow I_2}^{I_1} \rightarrow \gamma_{I_2 \rightarrow I_3}^{I_2} \rightarrow \cdots \rightarrow \gamma_{I_N \rightarrow I_{N+1}}^{I_N}, \quad (\text{A13})$$

where $\gamma_{I \rightarrow J}^I$ is the snippet of the full trajectory between two subsequent observable transitions I and J with waiting time t in between. This snippet starts in the destination state of I and ends immediately after the transition event J in the corresponding destination state. Since a given snippet is completed immediately after an observed transition J is registered for the first time, each trajectory snippet can be interpreted as a trajectory of an effective Markovian absorbing dynamics defined on the full network obtained by removing all observed links. As soon as the original trajectory ζ completes an observed transition, the absorbing dynamics for γ are terminated immediately. The corresponding first-passage time is precisely the length of γ in

time and corresponds to the waiting time t between two transitions in the effective description.

Practically, the effective absorbing Markov network is obtained from the corresponding original network by treating all observable links as absorbing, i.e., redirecting the observed transitions into absorbing states. An example for such an effective absorbing Markov network is shown in Fig. 5(c), which depicts the absorbing network for the effective description of the two-cycle network in Fig. 5(a). The possible transitions along the observed link are represented by the states (32) and (23), which are absorbing states in the associated first-passage problem. If the considered snippet begins with (23) or (32), the corresponding absorbing dynamics starts in 3 or 2, respectively.

The effective trajectory Γ originates from a mapping of microscopic trajectories $\zeta \rightarrow \Gamma[\zeta]$ to the effective description of the system. The path weight of Γ is obtained by summing over microscopic path weights

$$\mathcal{P}[\Gamma(t)|I_1, 0] = \sum_{\zeta \in \Gamma} \mathcal{P}[\zeta(t)|l_1, 0], \quad (\text{A14})$$

where $\mathcal{P}[\zeta|j_1, 0]$ is conditioned on l_1 at time $t = 0$ for $I_1 = (k_1 l_1)$. While integrating out the Markov path weight $\mathcal{P}[\zeta(t)]$ directly to obtain the coarse-grained path weight $\mathcal{P}[\Gamma(t)|I_1, 0]$ is not feasible, in general, the decomposition of Γ in Eq. (A9) and of ζ in Eq. (A13) reduces the problem

to the level of elementary building blocks $\psi_{I \rightarrow J}(t)$ and γ , respectively. Thus, the decomposition Eq. (A9) can be combined with the summation in Eq. (A14) to obtain

$$\mathcal{P}[\Gamma(t)|I_1, 0] = \psi_{I_1 \rightarrow I_2}(t_1) \psi_{I_2 \rightarrow I_3}(t_2) \cdots \psi_{I_N \rightarrow I_{N+1}}(t_N) \quad (\text{A15})$$

$$\begin{aligned} &= \sum_{\gamma \in \psi_{I_1 \rightarrow I_2}(t_1)} \mathcal{P}[\gamma|I_1, 0] \sum_{\gamma \in \psi_{I_2 \rightarrow I_3}(t_2)} \mathcal{P}[\gamma|I_2, 0] \\ &\cdots \sum_{\gamma \in \psi_{I_N \rightarrow I_{N+1}}(t_N)} \mathcal{P}[\gamma|I_N, 0]. \end{aligned} \quad (\text{A16})$$

The path weights $\mathcal{P}[\gamma|I_n, 0]$ of individual snippets $\gamma = \gamma_{I \rightarrow J}^t$ are seamlessly conditioned on the final state of their predecessor, since $I_n = (k_n l_n)$. The only type of summation that needs to be performed is the calculation of the waiting time distributions $\psi_{I \rightarrow J}(t)$ conditioned on $I = (kl)$ as introduced in Eq. (A10) by integrating all possible $\gamma = \gamma_{I \rightarrow J}^t$:

$$\psi_{I \rightarrow J}(t) = \sum_{\gamma \in \psi_{I \rightarrow J}(t)} \mathcal{P}[\gamma_{I \rightarrow J}^t|I, 0]. \quad (\text{A17})$$

This equation identifies the waiting time distributions of the effective description as summations over not observable trajectory snippets and proves, therefore, Eq. (4) in the main text.

For $I = (kl)$ and $J = (mn)$, $\gamma_{I \rightarrow J}^t$ starts at l and ends with a jump (mn) exactly at time t . Since the system is in m immediately before the jump at t , we can use the Markov property to calculate

$$\psi_{I \rightarrow J}(t) = P[\text{jump}(mn) \text{ at time } t|l, 0] \quad (\text{A18})$$

$$= P[\text{jump}(mn) \text{ at time } t|m, t]P(m, t|l, 0) \quad (\text{A19})$$

$$= k_{mn}p_m(t), \quad (\text{A20})$$

where Eq. (A4) is used for the last equality. The result in Eq. (A20) makes it possible to calculate waiting time distributions analytically by solving the master equation of the effective absorbing dynamics defined on the hidden subnetwork. Note that this procedure is, in principle, equivalent to calculating the first-passage time distributions for the associated first-passage problem with the method introduced in Ref. [76].

Conceptually, the reasoning used to derive Eq. (A17) and, therefore, Eq. (A20) is identical to the reasoning used in Ref. [61] to derive the intertransition time densities. For both derivations, the partially accessible Markov network considered in the transition-based description is mapped to an effective first-passage time problem and the waiting time distributions are identified as the corresponding first-passage

time distributions. In our derivation, this mapping is motivated from an effective splitting emerging on the level of single trajectories, whereas in the derivation in Ref. [61], the mapping is deduced mathematically.

Operationally, the proposed calculation method for waiting time distributions differs from the method proposed in Ref. [61]. Instead of carrying out the summation in Eq. (A20) explicitly, the waiting time distributions can be calculated from the solution of the effective absorbing master equation for different initial configurations using Eq. (A17). In addition, our calculation method is effective, since collecting histogram data from a Gillespie simulation [75] is unnecessary to reconstruct the waiting time distributions, as they can be calculated directly.

To give an explicit example, the proposed method is used to calculate the waiting time distributions for the effective description of the two-cycle network in Fig. 5(a). Solving the corresponding effective absorbing master equation for fixed, randomly drawn transition rates results in four different waiting time distributions; one of them is shown in Fig. 5(d). Additionally, the figure shows how this waiting time distribution based on Eq. (A20) coincides with the corresponding waiting time distribution calculated from histogram data simulated with a Gillespie algorithm of the full network for long trajectories.

APPENDIX B: ENTROPY ESTIMATOR

1. Coarse-grained and full entropy production

Our effective description loses information about irreversibility and entropy production. From an abstract point of view, a well-defined many-to-one mapping of trajectories $\zeta \mapsto \Gamma[\zeta]$ of length T suffices to bound the mean coarse-grained entropy production rate $\langle \hat{\sigma} \rangle$ against the physical entropy production rate $\langle \sigma \rangle$:

$$\langle \hat{\sigma} \rangle \equiv \frac{1}{T} \left\langle \ln \frac{\mathcal{P}[\Gamma]}{\mathcal{P}[\tilde{\Gamma}]} \right\rangle = \frac{1}{T} \sum_{\Gamma} \mathcal{P}[\Gamma] \ln \frac{\mathcal{P}[\Gamma]}{\mathcal{P}[\tilde{\Gamma}]} \leq \langle \sigma \rangle, \quad (\text{B1})$$

provided that $\Gamma \mapsto \tilde{\Gamma}$ is the correct, physical time-reversal operation. Technically, the bound relies on the log-sum inequality, a standard tool in information theory [77] stating

$$\sum_i a_i \ln \frac{\sum_i a_i}{\sum_i b_i} \leq \sum_i a_i \ln \frac{a_i}{b_i}, \quad (\text{B2})$$

for $a_i \geq 0$, $b_i \geq 0$. We apply this inequality in the form [27,78]

$$\begin{aligned} T \langle \hat{\sigma} \rangle &= \sum_{\zeta, \Gamma} \mathcal{P}[\Gamma|\zeta] \mathcal{P}[\zeta] \ln \frac{\sum_{\zeta'} \mathcal{P}[\Gamma|\zeta'] \mathcal{P}[\zeta]}{\sum_{\zeta'} \mathcal{P}[\tilde{\Gamma}|\zeta'] \mathcal{P}[\zeta]} \\ &\leq \sum_{\zeta, \Gamma} \mathcal{P}[\Gamma|\zeta] \mathcal{P}[\zeta] \ln \frac{\mathcal{P}[\Gamma|\zeta] \mathcal{P}[\zeta]}{\mathcal{P}[\tilde{\Gamma}|\zeta] \mathcal{P}[\zeta]} \end{aligned} \quad (\text{B3})$$

$$= \sum_{\zeta, \Gamma} \mathcal{P}[\Gamma|\zeta] \mathcal{P}[\zeta] \left(\ln \frac{\mathcal{P}[\Gamma|\zeta]}{\mathcal{P}[\tilde{\Gamma}|\zeta]} + \ln \frac{\mathcal{P}[\zeta]}{\mathcal{P}[\tilde{\zeta}]} \right) = T \langle \sigma \rangle. \quad (\text{B4})$$

The last equality follows since $\mathcal{P}[\Gamma|\zeta] = 1$ is satisfied only if Γ matches the correct effective trajectory $\Gamma[\zeta]$ and vanishes otherwise, $\mathcal{P}[\Gamma|\zeta] = 0$. Moreover, the equality requires that the first term in the sum vanishes, i.e., requires $\mathcal{P}[\tilde{\Gamma}|\tilde{\zeta}] = 1$ when $\mathcal{P}[\Gamma|\zeta] = 1$. This condition defines the modified time-reversal operation $\Gamma \mapsto \tilde{\Gamma}$ uniquely, since the correct $\tilde{\Gamma}$ is identified as the trajectory obtained by using $\xi = \tilde{\zeta}$ in the mapping $\xi \mapsto \Gamma[\xi]$. In other words, we have to first time reverse ζ , which is then followed by the coarse-graining operation, as discussed in Ref. [59].

2. Time reversal and conditional counting entropy estimator

The previous section identifies the correct time-reversal operation $\Gamma \mapsto \tilde{\Gamma}$ as the coarse-graining applied to the microscopic time reverse $\tilde{\zeta}(t) = \zeta(T-t)$. An effective trajectory Γ consists of a series of transitions $I_n = (k_n l_n)$ at times T_n , which is schematically denoted

$$\Gamma = (k_1 l_1) \xrightarrow{t_1} (k_2 l_2) \xrightarrow{t_2} (k_3 l_3) \xrightarrow{t_3} \dots \xrightarrow{t_{N-1}} (k_N l_N) \xrightarrow{t_N} (k_{N+1} l_{N+1}). \quad (\text{B5})$$

Compared to Eq. (A7), the jumping times T_i are replaced by the waiting times $t_i = T_i - T_{i-1}$ with $T_0 = 0$. Reversing the corresponding microscopic trajectory ζ in accordance with the previous discussion gives a well-defined effective trajectory of the form

$$\begin{aligned} \tilde{\Gamma} &= (l_{N+1} k_{N+1}) \xrightarrow{t_N} (l_N k_N) \xrightarrow{t_{N-1}} \dots \xrightarrow{t_3} (l_3 k_3) \xrightarrow{t_2} (l_2 k_2) \xrightarrow{t_1} (l_1 k_1) \\ &= \tilde{I}_{N+1} \xrightarrow{t_N} \tilde{I}_N \xrightarrow{t_{N-1}} \dots \xrightarrow{t_3} \tilde{I}_3 \xrightarrow{t_2} \tilde{I}_2 \xrightarrow{t_1} \tilde{I}_1, \end{aligned} \quad (\text{B6})$$

where we introduce the reversal operation on individual transitions $\tilde{I}_n \equiv (l_n k_n)$ for $I_n = (k_n l_n)$. The reverse transition happens along the same link and is, therefore, also observable in the effective description by construction. The path weight for the backward trajectory Eq. (B6) can be decomposed into a product of single waiting time distribution objects as in Eq. (A9):

$$\mathcal{P}[\tilde{\Gamma}(t)|I_{N+1}, 0] = P[\tilde{I}_N, T_N - T_{N-1} | \tilde{I}_{N+1}, 0] P[\tilde{I}_{N-1}, T_N - T_{N-2} | \tilde{I}_N, T_N - T_{N-1}] \dots P[\tilde{I}_1, T_N | \tilde{I}_2, T_N - T_1] \quad (\text{B7})$$

$$= \psi_{\tilde{I}_{N+1} \rightarrow \tilde{I}_N}(t_N) \psi_{\tilde{I}_N \rightarrow \tilde{I}_{N-1}}(t_{N-1}) \dots \psi_{\tilde{I}_2 \rightarrow \tilde{I}_1}(t_1). \quad (\text{B8})$$

After the proper time reverse $\tilde{\Gamma}$ is identified, the entropy production of a particular trajectory Γ can be calculated explicitly as

$$T \hat{\sigma} = \ln \frac{P[\Gamma]}{P[\tilde{\Gamma}]} = \ln \frac{P(I_1)}{P(\tilde{I}_{N+1})} + \ln \frac{\mathcal{P}[\Gamma|I_1, 0]}{\mathcal{P}[\tilde{\Gamma}|\tilde{I}_{N+1}, 0]} \quad (\text{B9})$$

$$= \ln \frac{P(I_1)}{P(\tilde{I}_{N+1})} + \sum_{j=1}^N \ln \frac{\psi_{I_j \rightarrow I_{j+1}}(t_j)}{\psi_{\tilde{I}_{j+1} \rightarrow \tilde{I}_j}(t_j)} \quad (\text{B10})$$

$$= \ln \frac{P(I_1)}{P(\tilde{I}_{N+1})} + T \sum_{I, J} \int_0^\infty dt \nu_{J|I}(t) \ln \frac{\psi_{I \rightarrow J}(t)}{\psi_{\tilde{J} \rightarrow \tilde{I}}(t)}, \quad (\text{B11})$$

where the conditional counters $\nu_{J|I}(t)$ are introduced as

$$\nu_{J|I}(t) \equiv \frac{1}{T} \sum_{j=1}^N \delta(t_j - t) \delta_{I_{j+1}, J} \delta_{I_j, I}. \quad (\text{B12})$$

In the limit $T \rightarrow \infty$, contributions from the initial and final states can be neglected, which yields the fluctuation theorem

$$\hat{\sigma} = \lim_{T \rightarrow \infty} \frac{1}{T} \ln \frac{P[\Gamma]}{P[\tilde{\Gamma}]} = \sum_{I, J} \int_0^\infty dt \langle \nu_{J|I}(t) \rangle \ln \frac{\psi_{I \rightarrow J}(t)}{\psi_{\tilde{J} \rightarrow \tilde{I}}(t)} \quad (\text{B13})$$

and an explicit formula for the expected coarse-grained entropy production rate

$$\langle \hat{\sigma} \rangle = \sum_{I, J} \int_0^\infty dt \langle \nu_{J|I}(t) \rangle \ln \frac{\psi_{I \rightarrow J}(t)}{\psi_{\tilde{J} \rightarrow \tilde{I}}(t)}. \quad (\text{B14})$$

3. Expectation values and entropy production for semi-Markov processes

We calculate the expectation value $\langle \nu_{J|I}(t) \rangle$ in Eq. (B14) using an appropriate technique known for semi-Markov processes. Note that the transitions I, J, \dots are the "states" of the semi-Markov process and that the waiting time t "in state I " is interpreted as the elapsed time since transition I . As defined in the main text, the conditional counter $\nu_{I \rightarrow J}(t)$ measures the number of transitions J after a preceding transition I :

$$\nu_{I \rightarrow J}(t) \Delta t = \frac{\text{No. of } (IJ) \text{ jumps after waiting time } \in [t, t + \Delta t]}{T}, \quad (\text{B15})$$

$$\langle \nu_{I \rightarrow J}(t) \rangle = P(\text{jump to } J \text{ after waiting time } t | I) \frac{\langle \text{No. of jumps from } I \rangle}{T} \quad (\text{B16})$$

$$= \psi_{I \rightarrow J}(t) \langle n_I \rangle = \psi_{I \rightarrow J}(t) \frac{p_I^s}{\langle t \rangle}. \quad (\text{B17})$$

In the last line, we use

$$\langle n_I \rangle = \frac{\langle \text{No. of jumps from } I \rangle}{T} = \frac{\langle \text{No. of jumps from } I \rangle}{\langle \text{total No. of jumps} \rangle} \cdot \frac{\langle \text{total No. of jumps} \rangle}{T} = p_I^s \cdot \frac{1}{\langle t \rangle}, \quad (\text{B18})$$

where $\langle t \rangle$ is defined as the average waiting time between two semi-Markov transitions. The identification of the stationary distribution p_I^s is based on elementary results for discrete-time Markov chains, as the number of visits of a particular state I in a long trajectory $(I_1 I_2 \dots I_N)$ divided by N tends toward p_I^s as $N \rightarrow \infty$. Note that, although this distribution is related to the stationary distribution of the semi-Markov process itself, they are different even in the Markovian case [56].

Since the $\psi_{I \rightarrow J}(t)$ are normalized by virtue of Eq. (A12), we can integrate over t to obtain the expected flux $\langle n_{JI} \rangle$ from a semi-Markov state I to J as

$$\langle n_{JI} \rangle = \int_0^\infty dt \langle \nu_{I \rightarrow J}(t) \rangle = p_{IJ} \frac{p_I^s}{\langle t \rangle} = \langle n_I \rangle p_{IJ}. \quad (\text{B19})$$

The semi-Markov entropy production σ_{SM} is defined by Eq. (50) as the probability ratio of forward and backward trajectory under the time-reversal operation $\Gamma \mapsto \tilde{\Gamma}$. Thus, the calculations of the previous section B 2 starting from Eq. (B11) actually apply to the semi-Markov entropy production $\sigma_{\text{SM}} = \hat{\sigma}$. Substituting Eq. (B17) into Eq. (B14), we obtain

$$\langle \sigma_{\text{SM}} \rangle = \langle \hat{\sigma} \rangle = \sum_{I,J} \int_0^\infty dt \langle n_I \rangle \psi_{I \rightarrow J}(t) \ln \frac{\psi_{I \rightarrow J}(t)}{\psi_{\tilde{J} \rightarrow \tilde{I}}(t)} \quad (\text{B20})$$

for the semi-Markov entropy production. To put this expression into relation with the entropy production of the EMC, we apply the log-sum inequality after using Eq. (B17) to obtain

$$\begin{aligned} \langle \hat{\sigma} \rangle &\geq \frac{1}{\langle t \rangle} \sum_{I,J} p_I^s \left[\int_0^\infty dt \psi_{I \rightarrow J}(t) \right] \ln \frac{\int_0^\infty dt \psi_{I \rightarrow J}(t)}{\int_0^\infty dt \psi_{\tilde{J} \rightarrow \tilde{I}}(t)} \\ &= \frac{1}{\langle t \rangle} \sum_{I,J} p_I^s p_{IJ} \ln \frac{p_{IJ}}{p_{\tilde{J}\tilde{I}}} = \langle \sigma_{\text{EMC}} \rangle \end{aligned} \quad (\text{B21})$$

in accordance with Eq. (52).

4. Comparison to informed partial entropy production

a. Entropy estimators: Embedded Markov chain versus informed partial

In this section, we prove that

$$\langle \sigma_{\text{EMC}} \rangle = \langle \sigma_{\text{IP}} \rangle \quad (\text{B22})$$

in the one-link case, which implies $\langle \sigma_{\text{IP}} \rangle \leq \langle \hat{\sigma} \rangle$ by virtue of Eq. (B21). We prove the case of one observable link between the Markov states k and l , since the crucial relation Eq. (B27) and its proof can be generalized to multiple observed links following an analogous approach. For two states $+ = (kl)$ and $- = (lk)$, Eq. (B21) simplifies to

$$\begin{aligned} \langle \sigma_{\text{EMC}} \rangle &= \frac{1}{\langle t \rangle} (p_+^s p_{++} - p_-^s p_{--}) \ln \frac{p_{++}}{p_{--}} \\ &= (\langle n_{++} \rangle - \langle n_{--} \rangle) \ln \frac{\int_0^\infty dt \psi_{++}(t)}{\int_0^\infty dt \psi_{--}(t)}, \end{aligned} \quad (\text{B23})$$

where Eqs. (B17) and (A12) are used for the second equality. It can be verified that for any sequence of transitions, i.e., any trajectory, $n_{++} - n_{--}$ and $n_+ - n_-$ differ by at most 1 due to terminal effects of the first and last transition that become negligible in the long-time limit. Thus, $\langle n_{++} - n_{--} \rangle = \langle n_+ - n_- \rangle = j$ can be used to express $\langle \sigma_{\text{EMC}} \rangle$ as

$$\langle \sigma_{\text{EMC}} \rangle = j \ln \frac{\int_0^\infty dt \psi_{++}(t)}{\int_0^\infty dt \psi_{--}(t)}. \quad (\text{B24})$$

This expression is now in a form where it can be compared with the informed partial entropy production [44,45]

$$\langle \sigma_{\text{IP}} \rangle = j \ln \frac{p_k^{\text{st}} k_{kl}}{p_l^{\text{st}} k_{lk}} \quad (\text{B25})$$

at the same link (connecting the Markov states k and l). The stalling distribution \mathbf{p}^{st} is defined as the stationary state of

the hidden subnetwork, where the link $k \rightarrow l$ is removed entirely. Thus, if the original process is generated by

$$\mathbf{L}_{ij} \equiv k_{ji} - \left(\sum_i k_{ji} \right) \delta_{ij}, \quad (\text{B26})$$

the stalling distribution satisfies $\mathbf{L}^{\text{st}} \mathbf{p}^{\text{st}} = 0$, with a modified generator \mathbf{L}^{st} that is obtained from \mathbf{L} by setting $k_{kl} = k_{lk} = 0$. The same stalling distribution \mathbf{p}^{st} can be accessed operationally if k_{kl} and k_{lk} depend on an external parameter F via $k_{kl}(F)/k_{lk}(F) = \exp(F)k_{kl}(0)/k_{lk}(0)$. For $F = 0$, the rates match their original value: $k_{kl}(0) = k_{kl}$ and $k_{lk}(0) = k_{lk}$, respectively. Then, we can find the stalling distribution by sweeping over all values of F until we find the value F^{st} where the stationary current $j = p_k^{\text{st}} k_{kl}(F^{\text{st}}) - p_l^{\text{st}} k_{lk}(F^{\text{st}})$ vanishes. In a unicyclic process, this information is sufficient to infer the cycle affinity \mathcal{A} [45]; thus, both $\langle \sigma_{\text{IP}} \rangle$ and $\langle \hat{\sigma} \rangle$ recover the full entropy production $\langle \sigma \rangle = j\mathcal{A}$ in this case. The relationship of the stalling distribution and the corresponding waiting-time quotient can be rooted on a more general level. As we prove,

$$\frac{p_k^{\text{st}} k_{kl}}{p_l^{\text{st}} k_{lk}} = \frac{\int_0^\infty dt \psi_{\rightarrow\rightarrow+}(t)}{\int_0^\infty dt \psi_{\rightarrow\rightarrow-}(t)} \quad (\text{B27})$$

holds true in a general Markov network, which suffices to establish $\langle \sigma_{\text{IP}} \rangle = \langle \sigma_{\text{EMC}} \rangle \leq \langle \hat{\sigma} \rangle$ from Eqs. (B24) and (B25). In particular,

$$\begin{aligned} \ln \frac{\langle \int_0^\infty dt \nu_{\rightarrow\rightarrow+}(t) \rangle / \langle n_+ \rangle}{\langle \int_0^\infty dt \nu_{\rightarrow\rightarrow-}(t) \rangle / \langle n_- \rangle} &= \frac{\int_0^\infty dt \psi_{\rightarrow\rightarrow+}(t)}{\int_0^\infty dt \psi_{\rightarrow\rightarrow-}(t)} = \frac{p_k^{\text{st}} k_{kl}(0)}{p_l^{\text{st}} k_{lk}(0)} \\ &= \frac{k_{lk}(F) k_{kl}}{k_{kl}(F) k_{lk}} = -F, \end{aligned} \quad (\text{B28})$$

where Eq. (B17) is used for the first equality. This result establishes Eq. (32) in the main text.

b. Proof of Eq. (B27)

To establish Eq. (B27), we consider the absorbing problem from Appendix A with two absorbing states $+$ and $-$, which indicate an observed forward jump $k \rightarrow l$ and backward jump $l \rightarrow k$, respectively. In the notation of Appendix A, we have $+$ = (kl) and $-$ = (lk) . The absorbing problem can be seen as a discrete-time Markov chain with transition probabilities $p_{i \rightarrow j}$ given by

$$p_{i \rightarrow j} = \begin{cases} \frac{k_{kl}}{\sum_j k_{kj}} & \text{if } i = k, j = +, \\ \frac{k_{lk}}{\sum_j k_{lj}} & \text{if } i = l, j = -, \\ 0 & \text{if } i = \pm, \\ 0 & \text{if } i = k, j = l \text{ or } i = l, j = k, \\ \frac{k_{ij}}{\sum_j k_{ij}} & \text{else.} \end{cases} \quad (\text{B29})$$

Here, $i, j \in \{1, \dots, N, +, -\}$ can be any one of the N Markov states or the absorbing states \pm .

Since the states $+$ and $-$ are absorbing, the Markov chain ends in one of these states almost surely. The probability that the last state is $+$ or $-$ given the current state j is denoted $P(\pm|j)$. These probabilities are related to the waiting time distributions via

$$\int_0^\infty dt \psi_{\rightarrow\rightarrow+}(t) = P[+|(kl)] = P(+|l), \quad (\text{B30})$$

$$\int_0^\infty dt \psi_{\rightarrow\rightarrow-}(t) = P[-|(lk)] = P(-|k) \quad (\text{B31})$$

by virtue of Eq. (A12). To calculate $P(+|j)$ and $P(-|j) = 1 - P(+|j)$, we observe that these probabilities have to satisfy a linear system of equations

$$P(+|i) = \sum_j p_{i \rightarrow j} P(+|j), \quad (\text{B32})$$

with analogous equations for $P(-|j)$. It is sufficient to let $1 \leq j \leq N$, since $P(+|+) = P(-|-) = 1 - P(+|-) = 1 - P(-|+) = 1$. The system in Eq. (B32) can be recast in matrix form by adjusting the generator matrix \mathbf{L} slightly. We define $\tilde{\mathbf{L}}$ by setting the (k, l) th and (l, k) th elements of \mathbf{L} to zero, i.e.,

$$\tilde{\mathbf{L}}_{ij} \equiv \begin{cases} 0 & i = k, j = l \text{ or } i = l, j = k, \\ \mathbf{L}_{ij} & \text{else.} \end{cases} \quad (\text{B33})$$

Note that $\tilde{\mathbf{L}}$ is not the generator of a Markov process, as it is not column stochastic. After substituting Eq. (B29) into Eq. (B32) and multiplying both sides with $\sum_j k_{ij}$, we rearrange terms to obtain

$$\tilde{\mathbf{L}}^T \mathbf{p}_+ = -k_{kl} \mathbf{e}_k, \quad (\text{B34})$$

$$\tilde{\mathbf{L}}^T \mathbf{p}_- = -k_{lk} \mathbf{e}_l, \quad (\text{B35})$$

with the vectors $\mathbf{p}_\pm \equiv \sum_i P(\pm|i) \mathbf{e}_i$. Applying Cramer's rule, we can express the inverse matrix $\tilde{\mathbf{L}}^{-1}$ as

$$(\tilde{\mathbf{L}}^T)^{-1}_{ij} = \frac{\det[(\tilde{\mathbf{L}}^T)_{(j|i)}]}{\det \tilde{\mathbf{L}}^T} (-1)^{i+j} = \frac{\det \tilde{\mathbf{L}}_{(i|j)}}{\det \tilde{\mathbf{L}}} (-1)^{i+j}. \quad (\text{B36})$$

Here, $\mathbf{L}_{(j|i)}$ denotes the matrix obtained by removing the j th row and the i th column from $\tilde{\mathbf{L}}$. By multiplying Eqs. (B34) and (B35) with $\tilde{\mathbf{L}}^{-1}$, we obtain

$$P(+|l) = -k_{kl} \tilde{\mathbf{L}}^{-1}_{lk} = -k_{kl} \frac{\det \tilde{\mathbf{L}}_{(l|k)}}{\det \tilde{\mathbf{L}}} (-1)^{l+k}, \quad (\text{B37})$$

$$P(-|k) = -k_{lk} \tilde{\mathbf{L}}_{kl}^{-1} = -k_{lk} \frac{\det \tilde{\mathbf{L}}^{(k|l)}}{\det \tilde{\mathbf{L}}} (-1)^{k+l} \quad (\text{B38})$$

for the k th row of Eq. (B34) and the n th row of Eq. (B35), respectively. Dividing these equations, we obtain

$$\frac{P(+|l)}{P(-|k)} = \frac{k_{kl} \det \tilde{\mathbf{L}}^{(l|k)}}{k_{lk} \det \tilde{\mathbf{L}}^{(k|l)}}. \quad (\text{B39})$$

This equality can be compared to a relation connecting the stalling distribution \mathbf{p}^{st} to the generator \mathbf{L}^{st} :

$$\frac{\det \mathbf{L}^{\text{st}}_{(l|k)}}{\det \mathbf{L}^{\text{st}}_{(k|l)}} = \frac{p_k^{\text{st}}}{p_l^{\text{st}}}, \quad (\text{B40})$$

which is established in Appendix B in Ref. [45]. Comparing the matrices \mathbf{L}^{st} and $\tilde{\mathbf{L}}$ [cf. Eq. (B33)], we observe that they differ only in the (k, k) th and the (l, l) th element, since the absorbing states affect the escape rates in state k and l only. In particular, the minors

$$\det \mathbf{L}^{\text{st}}_{(l|k)} = \det \tilde{\mathbf{L}}_{(l|k)}, \quad (\text{B41})$$

$$\det \mathbf{L}^{\text{st}}_{(k|l)} = \det \tilde{\mathbf{L}}_{(k|l)} \quad (\text{B42})$$

coincide, since $\mathbf{L}^{\text{st}}_{(l|k)} = \tilde{\mathbf{L}}_{(l|k)}$ and similarly for interchanged $l \leftrightarrow k$. By using these identities and Eqs. (B30), (B31), (B39), and (B40), the claim in Eq. (B27) follows from

$$\frac{\int_0^\infty dt \psi_{\rightarrow\rightarrow\rightarrow}(t)}{\int_0^\infty dt \psi_{\rightarrow\rightarrow\leftarrow}(t)} = \frac{P(+|l)}{P(-|k)} = \frac{p_k^{\text{st}} k_{kl}}{p_l^{\text{st}} k_{lk}}. \quad (\text{B43})$$

APPENDIX C: CYCLE LENGTH ESTIMATION FROM WAITING TIME DISTRIBUTIONS

As shown in Appendix A, the waiting time distributions of an observed system can be determined by solving the absorbing master equation (A3) for the corresponding escape problem. Microscopic trajectories associated with a waiting time distribution of the form $\psi_{I \rightarrow J}(t)$ for transitions $I = (kl)$, $J = (mn)$ starting in l must reach m . As implied by Eq. (A2), the short-time behavior of the corresponding path weight encodes the number of transitions needed for the completion of this path.

1. Length of the shortest connection

The length N_1 of the shortest connection between l and m in the hidden subnetwork, i.e., the minimal number of hidden transitions, is a lower bound on the number of transitions of any trajectory from l to m . By virtue of Eq. (A2), we have the scaling

$$p_m(t) \sim t^{N_1} \quad (\text{C1})$$

for the solution $p_m(t)$ of the corresponding absorbing master equation for $p_l(0) = 1$ as $t \rightarrow 0$. With Eq. (A20), this carries over to

$$\psi_{I \rightarrow J}(t) \sim t^{N_1}. \quad (\text{C2})$$

To extract N_1 from $\psi_{I \rightarrow J}(t)$, we take the logarithm of Eq. (C2), which results in

$$\ln \psi_{I \rightarrow J}(t) \sim N_1 \ln t. \quad (\text{C3})$$

Thus, the derivative with respect to $\ln t$ scales as

$$\frac{d[\ln \psi_{I \rightarrow J}(t)]}{d(\ln t)} \sim N_1, \quad (\text{C4})$$

for small t , which ultimately gives

$$\lim_{t \rightarrow 0} \left(t \frac{d}{dt} \ln \psi_{I \rightarrow J}(t) \right) = N_1 \quad (\text{C5})$$

in the limit $t \rightarrow 0$. Note that the logarithmic derivative in Eq. (C4) is written out explicitly in Eq. (C5) to increase readability. Based on Eq. (C5), the length N_1 of the shortest connection between l and m can be estimated from the short-time limit of a given waiting time distribution for transitions $I = (kl)$ and $J = (mn)$.

2. Length of the second-shortest connection

The second-shortest connection between $I = (kl)$ and $J = (mn)$ can be estimated similarly by considering the short-time limit of the ratio of waiting time distributions. To this end, we calculate the number of links in the second-shortest connection between the Markov states l and m from a timescale separation. The logarithmic ratio of waiting time distributions $a_{I \rightarrow J}(t)$ is defined as

$$a_{I \rightarrow J}(t) = \ln \frac{\sum_{\gamma'_{l \rightarrow j}} \mathcal{P}[\gamma'_{l \rightarrow j} | I]}{\sum_{\gamma'_{j \rightarrow \tilde{l}}} \mathcal{P}[\gamma'_{j \rightarrow \tilde{l}} | \tilde{J}]}, \quad (\text{C6})$$

where $\gamma'_{l \rightarrow j}$ denotes the snippet of the underlying trajectory starting with I and ending with J after time t with corresponding conditioned path weight $\mathcal{P}[\gamma'_{l \rightarrow j} | I]$. As defined in the main text and in Appendix B 2, the tilde on a capital letter reverses the corresponding transition, e.g., $\tilde{I} = (lk)$ for $I = (kl)$.

In a first step, we divide the sets of all possible snippets $\gamma'_{l \rightarrow j}$ and their time-reversed counterparts $\gamma'_{j \rightarrow \tilde{l}}$ into two subsets corresponding to their number of jumps. Let n_γ denote the number of hidden transitions between the states l and m in the snippet $\gamma'_{j \rightarrow \tilde{l}}$. By definition of N_1 , we have $n_\gamma \geq N_1$, which allows us to write

$$a_{I \rightarrow J}(t) = \ln \frac{\sum_{N_1 \leq n_\gamma < N_2} \mathcal{P}[\gamma_{I \rightarrow J}^t | I] + \sum_{n_\gamma \geq N_2} \mathcal{P}[\gamma_{I \rightarrow J}^t | I]}{\sum_{N_1 \leq n_\gamma < N_2} \mathcal{P}[\gamma_{\tilde{J} \rightarrow \tilde{I}}^t | \tilde{J}] + \sum_{n_\gamma \geq N_2} \mathcal{P}[\gamma_{\tilde{J} \rightarrow \tilde{I}}^t | \tilde{J}]} \quad (\text{C7})$$

for a natural number $N_2 > N_1$ which, at this point, is arbitrary. By using Eq. (A2), we note that for small t the two sums scale as

$$\sum_{N_1 \leq n_\gamma < N_2} \mathcal{P}[\gamma_{I \rightarrow J}^t | I] \simeq t^{N_1} [1 + \mathcal{O}(t^{N_1+1})], \quad (\text{C8})$$

$$\sum_{n_\gamma \geq N_2} \mathcal{P}[\gamma_{I \rightarrow J}^t | I] \simeq t^{N_2} [1 + \mathcal{O}(t^{N_2+1})]. \quad (\text{C9})$$

Since reversing a path does not change the number of jumps, the sums in the denominator satisfy analogous scaling laws. We now choose N_2 as the largest number for which

$$a_0 = \ln \frac{\sum_{N_1 \leq n_\gamma < N_2} \mathcal{P}[\gamma_{I \rightarrow J}^t | I]}{\sum_{N_1 \leq n_\gamma < N_2} \mathcal{P}[\gamma_{\tilde{J} \rightarrow \tilde{I}}^t | \tilde{J}]} \quad (\text{C10})$$

is time independent. Such a number exists if the shortest connection of length N_1 is unique, since in this case $N_1 + 1$ is a valid choice. The reason is that, if only paths containing N_1 transitions between l and m are allowed, only one possible connection remains; i.e., a_0 is time independent, because the network becomes unicyclic effectively. This argument remains valid as long as N_2 is smaller than or equal to the length of the second-shortest connection. As soon as n_γ is large enough to allow for paths along the second connection, $a(t)$ becomes time dependent if the resulting hidden cycle has nonvanishing affinity.

Thus, we proceed knowing that N_2 as defined in Eq. (C10) is the length of the second-shortest connection. Substituting this equation into Eq. (C7), we obtain

$$a_{I \rightarrow J}(t) = a_0 + \ln \frac{1 + \sum_{n_\gamma \geq N_2} \mathcal{P}[\gamma_{I \rightarrow J}^t | I] / \sum_{N_1 \leq n_\gamma < N_2} \mathcal{P}[\gamma_{I \rightarrow J}^t | I]}{1 + \sum_{n_\gamma \geq N_2} \mathcal{P}[\gamma_{\tilde{J} \rightarrow \tilde{I}}^t | \tilde{J}] / \sum_{N_1 \leq n_\gamma < N_2} \mathcal{P}[\gamma_{\tilde{J} \rightarrow \tilde{I}}^t | \tilde{J}]} \quad (\text{C11})$$

After rearranging terms, we use Eqs. (C8) and (C9) to extract the lowest-order correction in the numerator:

$$\ln \left(1 + \frac{\sum_{n_\gamma \geq N_2} \mathcal{P}[\gamma_{I \rightarrow J}^t | I]}{\sum_{N_1 \leq n_\gamma < N_2} \mathcal{P}[\gamma_{I \rightarrow J}^t | I]} \right) \sim t^{N_2 - N_1}, \quad (\text{C12})$$

and similarly for the denominator. After rearranging terms in Eq. (C11),

$$\Delta a_{I \rightarrow J}(t) \equiv a_{I \rightarrow J}(t) - a_0 \sim t^{N_2 - N_1}, \quad (\text{C13})$$

and taking the limit $t \rightarrow 0$ yields the result

$$\lim_{t \rightarrow 0} \left(t \frac{d}{dt} \ln |\Delta a_{I \rightarrow J}(t)| \right) = N_2 - N_1. \quad (\text{C14})$$

APPENDIX D: MULTIPLE OBSERVED LINKS: FULL ENTROPY PRODUCTION IF HIDDEN NETWORK IS TRIVIAL

We now prove the second part of rule 1 in Sec. VB, which asserts that the full entropy production is recovered in the long-time limit $T \rightarrow \infty$, i.e.,

$$\langle \sigma \rangle = \langle \hat{\sigma} \rangle \quad (\text{D1})$$

if the hidden subnetwork is topologically trivial. We start by recalling the total medium entropy production s_m of a

Markov trajectory $\zeta = (n_0 n_1 \dots n_M)$ and its corresponding fluctuation theorem [3]

$$s_m[\zeta] \equiv \sum_{j=1}^M \ln \frac{k_{n_{j-1} n_j}}{k_{n_j n_{j-1}}} = \ln \frac{\mathcal{P}[\zeta(t) | n_0]}{\mathcal{P}[\tilde{\zeta}(t) | n_M]}. \quad (\text{D2})$$

In the long-time limit $T \rightarrow \infty$, it is known that

$$\langle \sigma \rangle = \frac{1}{T} \langle s_m \rangle, \quad (\text{D3})$$

since the difference between σ and s_m/T is a stochastic entropy term that is not extensive in time. Using the splitting introduced in Eq. (A13), the medium entropy production can be decomposed similarly, which is written here somewhat symbolically as

$$s_m[\zeta] = \sum_{j=1}^N \sigma_m[\gamma_{I_j \rightarrow I_{j+1}}^{t_j}] + \sum_{j=1}^{N+1} \ln \frac{k_{k_j l_j}}{k_{l_j k_j}}. \quad (\text{D4})$$

The second term contains the entropy production due to the visible transitions $I_j = (k_j l_j)$ ($j = 1, \dots, N+1$) with respective transition rates k_j and their reverse $k_{\tilde{j}}$. In contrast, the first term includes the exact medium entropy production of a trajectory snippet $\gamma_{I_j \rightarrow I_{j+1}}^{t_j}$ in the hidden subnetwork, i.e., without including the contributions from the visible initial and final transitions I_j and I_{j+1} , respectively.

Since the hidden subnetwork satisfies detailed balance, as it does not contain any hidden cycles, it is possible to identify a well-defined potential function $F(i)$ on the Markov states i satisfying

$$F(i) - F(j) = \ln \frac{k_{ij}}{k_{ji}} \quad (\text{D5})$$

for neighboring states i and j in the hidden subnetwork. With this potential function, the stochastic entropy production of a trajectory in the hidden subnetwork becomes path independent: A trajectory γ starting and ending in states l and k , respectively, satisfies $\sigma_m[\gamma] = F(l) - F(k)$. In particular, we can use the fluctuation theorem property Eq. (D4) of σ_m to identify

$$\begin{aligned} F(l_j) - F(k_{j+1}) &= s_m[\mathcal{Y}_{I_j \rightarrow I_{j+1}}^{l_j}] \\ &= \ln \frac{\mathcal{P}[\mathcal{Y}_{I_j \rightarrow I_{j+1}}^{l_j} | I_j]}{\mathcal{P}[\mathcal{Y}_{I_{j+1} \rightarrow \tilde{I}_j}^{l_j} | \tilde{I}_{j+1}]} - \ln \frac{k_{k_{j+1}l_{j+1}}}{k_{l_j k_j}}. \end{aligned} \quad (\text{D6})$$

Because of the existence of the potential, the result is independent of the particular sequence of transitions in $\mathcal{Y}_{I_j \rightarrow I_{j+1}}^{l_j}$. Note that the second term is needed, because the observed transitions that terminate a trajectory snippet are not accounted for in σ_m , which it is defined in the hidden subnetwork.

Since the hidden subnetwork is topologically trivial, we can evaluate the ratio of path weights in Eq. (D6) using Eq. (39). We obtain

$$a_{I_j I_{j+1}} = \ln \frac{\mathcal{P}[\mathcal{Y}_{I_j \rightarrow I_{j+1}}^{l_j} | I_j]}{\mathcal{P}[\mathcal{Y}_{I_{j+1} \rightarrow \tilde{I}_j}^{l_j} | \tilde{I}_{j+1}]} = s_m[\mathcal{Y}_{I_j \rightarrow I_{j+1}}^{l_j}] + \ln \frac{k_{k_{j+1}l_{j+1}}}{k_{l_j k_j}} \quad (\text{D7})$$

for the trajectory snippets between two observed jumps. Reassembling these individual contributions via Eq. (D4) yields

$$s_m[\zeta] = \sum_{j=1}^N a_{I_j I_{j+1}} + \ln \frac{k_{k_1 l_1}}{k_{l_{N+1} k_{N+1}}}. \quad (\text{D8})$$

The first term recovers the value of $\hat{\sigma}$ precisely, because Eq. (36) reduces to

$$\hat{\sigma} = \sum_{IJ} a_{IJ} n_{JI} = \frac{1}{T} \sum_{j=1}^N a_{I_j I_{j+1}}, \quad (\text{D9})$$

since $a_{IJ}(t) = a_{IJ}$ is time independent. To calculate the corresponding averages, we note that the second term in Eq. (D8) is negligible in the limit $T \rightarrow \infty$. By combining Eqs. (D3), (D8), and (D9), we conclude

$$\langle \sigma \rangle = \frac{1}{T} \langle s_m \rangle = \langle \hat{\sigma} \rangle. \quad (\text{D10})$$

This last equality verifies the claim in rule 1 in Sec. VB.

APPENDIX E: MODEL PARAMETERS, SIMULATION, AND COUNTEREXAMPLE

1. Unicyclic network for the illustration of the coarse-graining scheme in Fig. 1

The unicyclic network in Fig. 1 in the main text includes four different states with different links in between. The transition rates for the network are shown in Table I. The waiting time distributions shown in Fig. 1(d) in the main text can be derived from the solution of the absorbing master equation for the effective absorbing Markov network defined by Fig. 1(b) in the main text with the method from Appendix A. For the waiting time distributions shown in Fig. 1(d) in the main text, the corresponding absorbing master equation for the transition rates in Table I is solved numerically.

2. Multicyclic network for the illustration of the affinity bounds in Fig. 2

The multicyclic network in Fig. 2 in the main text includes seven different states with different links in between. The transition rates for the network leading to the affinities given in the caption of Fig. 2 in the main text are shown in Table II. This specific choice of transition rates results in different timescales for the transitions through the individual cycles including the observable link. Thus, no cycle is preferred, and the existence of all cycles can be inferred from the successive maxima and minima of the corresponding $a(t)$.

$a_{(71) \rightarrow (71)}(t)$ in Figs. 2(c) and 2(d) in the main text is by definition given by the logarithm of the fraction of the corresponding waiting time distributions. As discussed in Appendix A, these waiting time distributions can be derived from the solution of the absorbing master equation for the effective absorbing Markov network defined by Fig. 2(b) in the main text. For $a_{(71) \rightarrow (71)}(t)$ shown in Figs. 2(c) and 2(d) in the main text, the corresponding absorbing master equation for the transition rates in Table II is solved numerically.

TABLE I. Transition rates for the unicyclic network in Fig. 1.

State 1	State 2	State 3	State 4
$k_{12} = 1.2$	$k_{21} = 1.7$	$k_{31} = 1.0$	$k_{41} = 1.9$
$k_{13} = 3.6$	$k_{23} = 1.0$	$k_{32} = 1.0$	$k_{41} = 1.9$
$k_{14} = 2.0$		$k_{34} = 1.8$	

TABLE II. Transition rates for the multicyclic network in Fig. 2.

State 1	State 2	State 3	State 4	State 5	State 6	State 7
$k_{12} = 1.0$	$k_{21} = 1.0$	$k_{31} = 1.0$	$k_{43} = 5.0$	$k_{54} = 3.0$	$k_{65} = 1.0$	$k_{71} = 1.0$
$k_{13} = 3.0$	$k_{23} = 1.0$	$k_{32} = 8.0$	$k_{45} = 3.0$	$k_{56} = 4.0$	$k_{67} = 30.0$	$k_{72} = 0.1$
$k_{17} = 1.0$	$k_{27} = 0.1$	$k_{34} = 40.0$		$k_{57} = 0.5$		$k_{75} = 50.0$
						$k_{76} = 2.0$

TABLE III. Distributions of the random transition rates for the multicyclic network in Fig. 3. $\Theta(a, b)$ denotes a uniform distribution defined between a and b .

State 1	State 2	State 3	State 4	State 5	State 6	State 7
$k_{12} : \Theta(0.01, 80)$	$k_{21} : \Theta(0.01, 2)$	$k_{31} : \Theta(0.01, 2)$	$k_{43} : \Theta(0.01, 2)$	$k_{54} : \Theta(0.01, 2)$	$k_{65} : \Theta(0.01, 2)$	$k_{71} : \Theta(0.01, 80)$
$k_{13} : \Theta(0.01, 20)$	$k_{23} : \Theta(0.01, 80)$	$k_{32} : \Theta(0.01, 2)$	$k_{45} : \Theta(0.01, 20)$	$k_{56} : \Theta(0.01, 20)$	$k_{67} : \Theta(0.01, 20)$	$k_{72} : \Theta(0.01, 2)$
$k_{17} : \Theta(0.01, 2)$	$k_{27} : \Theta(0.01, 80)$	$k_{34} : \Theta(0.01, 20)$		$k_{57} : \Theta(0.01, 20)$		$k_{75} : \Theta(0.01, 20)$
						$k_{76} : \Theta(0.01, 20)$

3. Multicyclic network for the quality factors of the affinity bounds in Fig. 3

The multicyclic network from Fig. 2 in the main text is also used in Fig. 3 in the main text to illustrate the quality of the derived affinity bounds. For each realization of the network, the transition rates are drawn randomly according to the distributions given in Table III. All transition rates are distributed uniformly. The different choices for the definition intervals lead, on the one hand, to a bias in the affinity \mathcal{A}_{C_0} toward positive values and increase, on the other hand, the maximal possible value of \mathcal{A}_{C_0} aiming at a broad range of possible affinities for the scatter plots of the quality factors in Fig. 3 in the main text. As a consequence of this bias, it is more likely to draw high positive affinities rather than high negative ones. Since the bounds for the maximal affinities are tighter for single, high positive affinities, the quality factors \mathcal{Q}_+ in Fig. 3(c) are centered around higher values in comparison to the quality factors \mathcal{Q}_- in Fig. 3(d).

To calculate the quality factors for the two different classes of network configurations shown in Figs. 3(b)–3(d) in the main text, the maximum and minimum of $a_{(71) \rightarrow (71)}(t)$ are needed for all randomly drawn realization of the multicyclic network. For a given realization, $a_{(71) \rightarrow (71)}(t)$ can be calculated from the waiting time distributions that can be derived by using the absorbing master equation method from Appendix A. For each realization corresponding to one quality factor shown in Figs. 3(b)–3(d) in the main text, the absorbing master equation for the drawn transition rates is solved numerically, $a_{(71) \rightarrow (71)}(t)$ is determined, and the values of the maximum and minimum of $a_{(71) \rightarrow (71)}(t)$ are used to calculate the corresponding quality factor according to the definitions given in the caption of Fig. 3 in the main text.

4. Two-cycle network for topology and the entropy estimators in Fig. 4

The two-cycle network in Fig. 4 in the main text includes four different states and five links in total. Since the network is comparatively compact yet nontrivial, it is also used as an example network for multiple extant entropy estimators [39,42,44,45]. To compare the introduced entropy estimator $\hat{\sigma}$ to existing results, the rates given in Table IV are chosen according to the rates in Ref. [39]. The force parameter F applied to the observable link is related to the transition rates of the observed link via

$$-2F = \ln \frac{k_{23}}{k_{32}} - \ln \frac{2}{3}. \quad (\text{E1})$$

This parameter is introduced in Ref. [39] to tune the observed net current $j = n_+ - n_-$. To estimate the cycle lengths as discussed in Figs. 4(b) and 4(c) in the main text, the waiting time distributions for the observable transition are needed to calculate $\ln \psi_{(32) \rightarrow (32)}(t)$ and $a_{(32) \rightarrow (32)}(t)$. As for the networks in Figs. 1 and 2, these distributions can be derived by using the absorbing master equation method from Appendix A. For the estimations of the cycle lengths shown in Figs. 4(b) and 4(c), the corresponding absorbing master equation for the transition rates in Table II with $F = \ln 3$ is solved numerically.

TABLE IV. Transition rates for the two-cycle network in Fig. 4. F is a dimensionless force applied to the observable link between states 2 and 3.

State 1	State 2	State 3	State 4
$k_{12} = 1.0$	$k_{21} = 8.0$	$k_{31} = 0.2$	$k_{41} = 75.0$
$k_{13} = 35.0$	$k_{23} = 3.0 \cdot \exp(-F)$	$k_{32} = 2.0 \cdot \exp(F)$	$k_{43} = 2.0$
$k_{14} = 0.7$		$k_{34} = 50.0$	

To calculate the introduced entropy estimator $\hat{\sigma}$ for a given trajectory of the two-cycle network, $a(t)$ and the conditioned transition counters $\nu_{++}(t)$ and $\nu_{--}(t)$ of the observed link are needed. $a(t)$ can be calculated independently of $\nu_{++}(t)$ and $\nu_{--}(t)$ from the corresponding waiting time distributions derived with the absorbing master equation method from Appendix A. A trajectory resulting from the observation of the two-cycle network can be generated by simulating the full underlying Markov network with the Gillespie algorithm [75]. For the entropy estimator in Fig. 3(c), $a(t)$ is calculated from the waiting time distributions resulting from the numerical solution of the corresponding absorbing master equation. The conditioned transition counters are calculated by counting the corresponding transitions in a simulated Gillespie trajectory of length $T = 10^7$; weighting the calculated number of transitions with the corresponding $a(t)$ evaluated at the registered waiting time leads to $\langle \hat{\sigma} \rangle$. The mean entropy production of the Markov network is directly calculated in the Gillespie simulation.

5. A model with an invisible cycle

In this section, we present an explicit Markov network that has a cycle with nonvanishing affinity in the hidden subnetwork, although all $a_{IJ}(t)$ are time independent. We use the network in Fig. 4 with the choice of rates given by Table V. Instead of observing the transitions between states 2 and 3, we observe $I_+ = (13)$ and $I_- = (31)$.

This network has the remarkable property that lumping states 2 and 4 into a single compound state H results in a Markov network. The new transition rates are given by

$$k_{1H} = k_{12} + k_{14} = x + 1, \quad (\text{E2})$$

$$k_{3H} = k_{32} + k_{34} = 2, \quad (\text{E3})$$

$$k_{H1} = k_{21} = k_{41} = 1, \quad (\text{E4})$$

$$k_{H3} = k_{23} = k_{43} = 1. \quad (\text{E5})$$

The ratio $a(t)$ remains unaffected by this procedure. In particular, since the model is now reduced to a unicyclic network with cycle $\mathcal{C} = (13H1)$, $a(t)$ is constant in time, taking the value $a(t) = \mathcal{A}_{\mathcal{C}} = \ln[2/(a+1)]$. In contrast, the cycle affinity of the true hidden cycle $\mathcal{C}' = (12341)$ in

the hidden subnetwork is given by $\mathcal{A}_{\mathcal{C}'} = \ln a$. For $a \neq 1$, this model is an example for which $a(t)$ is constant in time despite the presence of a cycle with nonvanishing affinity in the hidden subnetwork.

-
- [1] K. Sekimoto, *Stochastic Energetics*, Lecture Notes in Physics (Springer, Berlin, 2010).
 - [2] C. Jarzynski, *Equalities and Inequalities: Irreversibility and the Second Law of Thermodynamics at the Nanoscale*, *Annu. Rev. Condens. Matter Phys.* **2**, 329 (2011).
 - [3] U. Seifert, *Stochastic Thermodynamics, Fluctuation Theorems and Molecular Machines*, *Rep. Prog. Phys.* **75**, 126001 (2012).
 - [4] C. V. d. Broeck and M. Esposito, *Ensemble and Trajectory Thermodynamics: A Brief Introduction*, *Physica (Amsterdam)* **418A**, 6 (2015).
 - [5] L. Peliti and S. Pigolotti, *Stochastic Thermodynamics—An Introduction* (Princeton University Press, Princeton, NJ, 2021).
 - [6] T. Schmiedl and U. Seifert, *Stochastic Thermodynamics of Chemical Reaction Networks*, *J. Chem. Phys.* **126**, 044101 (2007).
 - [7] H. Ge, M. Qian, and H. Qian, *Stochastic Theory of Non-equilibrium Steady States. Part II: Applications in Chemical Biophysics*, *Phys. Rep.* **510**, 87 (2012).
 - [8] R. Rao and M. Esposito, *Nonequilibrium Thermodynamics of Chemical Reaction Networks: Wisdom from Stochastic Thermodynamics*, *Phys. Rev. X* **6**, 041064 (2016).
 - [9] T. E. Ouldridge, C. C. Govern, and P. R. ten Wolde, *Thermodynamics of Computational Copying in Biochemical Systems*, *Phys. Rev. X* **7**, 021004 (2017).
 - [10] R. Marsland, W. Cui, and J. M. Horowitz, *The Thermodynamic Uncertainty Relation in Biochemical Oscillations*, *J. R. Soc. Interface* **16**, 20190098 (2019).
 - [11] G. R. Bowman and V. S. Pande, *Protein Folded States Are Kinetic Hubs*, *Proc. Natl. Acad. Sci. U.S.A.* **107**, 10890 (2010).
 - [12] J. Stigler, F. Ziegler, A. Gieseke, J. C. M. Gebhardt, and M. Rief, *The Complex Folding Network of Single Calmodulin Molecules*, *Science* **334**, 512 (2011).
 - [13] J. D. Chodera and F. Noé, *Markov State Models of Biomolecular Conformational Dynamics*, *Curr. Opin. Struct. Biol.* **25**, 135 (2014).
 - [14] H. Qian, *A simple theory of motor protein kinetics and energetics*, *Biophys. Chem.* **67**, 263 (1997).
 - [15] D. Andrieux and P. Gaspard, *Fluctuation Theorems and the Nonequilibrium Thermodynamics of Molecular Motors*, *Phys. Rev. E* **74**, 011906 (2006).
 - [16] S. Liepelt and R. Lipowsky, *Kinesin's Network of Chemo-mechanical Motor Cycles*, *Phys. Rev. Lett.* **98**, 258102 (2007).
 - [17] D. Chowdhury, *Stochastic Mechano-chemical Kinetics of Molecular Motors: A Multidisciplinary Enterprise from a Physicist's Perspective*, *Phys. Rep.* **529**, 1 (2013).
 - [18] J. A. Wagoner and K. A. Dill, *Molecular Motors: Power Strokes Outperform Brownian Ratchets*, *J. Phys. Chem. B* **120**, 6327 (2016).

TABLE V. Transition rates for the counterexample. The network is given by Fig. 4 with the specified configuration of rates.

State 1	State 2	State 3	State 4
$k_{12} = x$	$k_{21} = 1.0$	$k_{31} = 1.0$	$k_{41} = 1.0$
$k_{13} = 1.0$	$k_{23} = 1.0$	$k_{32} = 1.0$	$k_{43} = 1.0$
$k_{14} = 1.0$		$k_{34} = 1.0$	

- [19] T. Speck, *Modeling of Biomolecular Machines in Non-equilibrium Steady States*, *J. Chem. Phys.* **155**, 230901 (2021).
- [20] J.-H. Prinz, H. Wu, M. Sarich, B. Keller, M. Senne, M. Held, J. D. Chodera, C. Schütte, and F. Noé, *Markov Models of Molecular Kinetics: Generation and Validation*, *J. Chem. Phys.* **134**, 174105 (2011).
- [21] B. E. Husic and V. S. Pande, *Markov State Models: From an Art to a Science*, *J. Am. Chem. Soc.* **140**, 2386 (2018).
- [22] W. Wang, S. Cao, L. Zhu, and X. Huang, *Constructing Markov State Models to Elucidate the Functional Conformational Changes of Complex Biomolecules*, *Comput. Mol. Sci.* **8**, e1343 (2018).
- [23] A. C. Barato and U. Seifert, *Thermodynamic Uncertainty Relation for Biomolecular Processes*, *Phys. Rev. Lett.* **114**, 158101 (2015).
- [24] T. R. Gingrich, J. M. Horowitz, N. Perunov, and J. L. England, *Dissipation Bounds All Steady-State Current Fluctuations*, *Phys. Rev. Lett.* **116**, 120601 (2016).
- [25] J. M. Horowitz and T. R. Gingrich, *Thermodynamic Uncertainty Relations Constrain Non-equilibrium Fluctuations*, *Nat. Phys.* **16**, 15 (2020).
- [26] W. Hwang and C. Hyeon, *Energetic Costs, Precision, and Transport Efficiency of Molecular Motors*, *J. Phys. Chem. Lett.* **9**, 513 (2018).
- [27] U. Seifert, *From Stochastic Thermodynamics to Thermodynamic Inference*, *Annu. Rev. Condens. Matter Phys.* **10**, 171 (2019).
- [28] J. Li, J. M. Horowitz, T. R. Gingrich, and N. Fakhri, *Quantifying Dissipation Using Fluctuating Currents*, *Nat. Commun.* **10**, 1666 (2019).
- [29] Y. Song and C. Hyeon, *Thermodynamic Cost, Speed, Fluctuations, and Error Reduction of Biological Copy Machines*, *J. Phys. Chem. Lett.* **11**, 3136 (2020).
- [30] T. Van Vu, V. T. Vo, and Y. Hasegawa, *Entropy Production Estimation with Optimal Current*, *Phys. Rev. E* **101**, 042138 (2020).
- [31] A. Dechant and S. I. Sasa, *Improving Thermodynamic Bounds Using Correlations*, *Phys. Rev. X* **11**, 041061 (2021).
- [32] A. C. Barato and U. Seifert, *Universal Bound on the Fano Factor in Enzyme Kinetics*, *J. Phys. Chem. B* **119**, 6555 (2015).
- [33] P. Pietzonka, A. C. Barato, and U. Seifert, *Affinity- and Topology-Dependent Bound on Current Fluctuations*, *J. Phys. A* **49**, 34LT01 (2016).
- [34] R. Kawai, J. M. R. Parrondo, and C. Van den Broeck, *Dissipation: The Phase-Space Perspective*, *Phys. Rev. Lett.* **98**, 080602 (2007).
- [35] J. M. R. Parrondo, C. V. d. Broeck, and R. Kawai, *Entropy Production and the Arrow of Time*, *New J. Phys.* **11**, 073008 (2009).
- [36] E. Roldán and J. M. R. Parrondo, *Estimating Dissipation from Single Stationary Trajectories*, *Phys. Rev. Lett.* **105**, 150607 (2010).
- [37] E. Roldán and J. M. R. Parrondo, *Entropy Production and Kullback-Leibler Divergence between Stationary Trajectories of Discrete Systems*, *Phys. Rev. E* **85**, 031129 (2012).
- [38] S. Mui, A. Kundu, and D. Lacoste, *Non-invasive Estimation of Dissipation from Non-equilibrium Fluctuations in Chemical Reactions*, *J. Chem. Phys.* **139**, 124109 (2013).
- [39] I. A. Martínez, G. Bisker, J. M. Horowitz, and J. M. R. Parrondo, *Inferring Broken Detailed Balance in the Absence of Observable Currents*, *Nat. Commun.* **10**, 3542 (2019).
- [40] D. J. Skinner and J. Dunkel, *Improved Bounds on Entropy Production in Living Systems*, *Proc. Natl. Acad. Sci. U.S.A.* **118**, e2024300118 (2021).
- [41] D. J. Skinner and J. Dunkel, *Estimating Entropy Production from Waiting Time Distributions*, *Phys. Rev. Lett.* **127**, 198101 (2021).
- [42] J. Ehrich, *Tightest Bound on Hidden Entropy Production from Partially Observed Dynamics*, *J. Stat. Mech.* (2021) 083214.
- [43] N. Shiraishi and T. Sagawa, *Fluctuation Theorem for Partially Masked Nonequilibrium Dynamics*, *Phys. Rev. E* **91**, 012130 (2015).
- [44] M. Poletini and M. Esposito, *Effective Thermodynamics for a Marginal Observer*, *Phys. Rev. Lett.* **119**, 240601 (2017).
- [45] G. Bisker, M. Poletini, T. R. Gingrich, and J. M. Horowitz, *Hierarchical Bounds on Entropy Production Inferred from Partial Information*, *J. Stat. Mech.* (2017) 093210.
- [46] S. Rahav and C. Jarzynski, *Fluctuation Relations and Coarse-Graining*, *J. Stat. Mech.* (2007) P09012.
- [47] S. Pigolotti and A. Vulpiani, *Coarse Graining of Master Equations with Fast and Slow States*, *J. Chem. Phys.* **128**, 154114 (2008).
- [48] A. Puglisi, S. Pigolotti, L. Rondoni, and A. Vulpiani, *Entropy Production and Coarse Graining in Markov Processes*, *J. Stat. Mech.* (2010) P05015.
- [49] F. Knoch and T. Speck, *Cycle Representatives for the Coarse-Graining of Systems Driven into a Non-equilibrium Steady State*, *New J. Phys.* **17**, 115004 (2015).
- [50] D. Seifert, P. Sollich, and S. Klumpp, *Coarse Graining of Biochemical Systems Described by Discrete Stochastic Dynamics*, *Phys. Rev. E* **102**, 062149 (2020).
- [51] M. Esposito, *Stochastic Thermodynamics under Coarse Graining*, *Phys. Rev. E* **85**, 041125 (2012).
- [52] J. Mehl, B. Lander, C. Bechinger, V. Blickle, and U. Seifert, *Role of Hidden Slow Degrees of Freedom in the Fluctuation Theorem*, *Phys. Rev. Lett.* **108**, 220601 (2012).
- [53] S. Bo and A. Celani, *Entropy Production in Stochastic Systems with Fast and Slow Time-scales*, *J. Stat. Phys.* **154**, 1325 (2014).
- [54] S. Bo and A. Celani, *Multiple-Scale Stochastic Processes: Decimation, Averaging and beyond*, *Phys. Rep.* **670**, 1 (2017).
- [55] M. Uhl, P. Pietzonka, and U. Seifert, *Fluctuations of Apparent Entropy Production in Networks with Hidden Slow Degrees of Freedom*, *J. Stat. Mech.* (2018) 023203.
- [56] H. Wang and H. Qian, *On Detailed Balance and Reversibility of Semi-Markov Processes and Single-Molecule Enzyme Kinetics*, *J. Math. Phys. (N.Y.)* **48**, 013303 (2007).
- [57] G. Teza and A. L. Stella, *Exact Coarse Graining Preserves Entropy Production out of Equilibrium*, *Phys. Rev. Lett.* **125**, 110601 (2020).
- [58] B. Ertel, J. van der Meer, and U. Seifert, *Operationally Accessible Uncertainty Relations for Thermodynamically*

- Consistent Semi-Markov Processes*, *Phys. Rev. E* **105**, 044113 (2022).
- [59] D. Hartich and A. Godec, *Emergent Memory and Kinetic Hysteresis in Strongly Driven Networks*, *Phys. Rev. X* **11**, 041047 (2021).
- [60] D. Hartich and A. Godec, *Violation of Local Detailed Balance despite a Clear Time-scale Separation*, [arXiv:2111.14734](https://arxiv.org/abs/2111.14734).
- [61] P. E. Harunari, A. Dutta, M. Poletini, and Édgar Roldán, *What to Learn from Few Visible Transitions' Statistics?*, [arXiv:2203.07427](https://arxiv.org/abs/2203.07427).
- [62] J. Schnakenberg, *Network Theory of Microscopic and Macroscopic Behavior of Master Equation Systems*, *Rev. Mod. Phys.* **48**, 571 (1976).
- [63] T. L. Hill, *Free Energy Transduction and Biochemical Cycle Kinetics* (Springer, New York, 1989).
- [64] Typically, the expected net number of completed cycles j_C does not coincide with any current through an edge contained in the cycle. In particular, j_C does not rely on the identification of spanning trees or fundamental cycles but is well defined after specifying \mathcal{C} in a particular network as explained in Ref. [65].
- [65] D.-Q. Jiang, M. Qian, and M.-P. Qian, *Mathematical Theory of Nonequilibrium Steady States* (Springer, Berlin, 2004).
- [66] D. Hartich and A. Godec, *Comment on "Inferring Broken Detailed Balance in the Absence of Observable Currents,"* [arXiv:2112.08978](https://arxiv.org/abs/2112.08978).
- [67] G. Bisker, I. A. Martínez, J. M. Horowitz, and J. M. R. Parrondo, *Comment on "Inferring Broken Detailed Balance in the Absence of Observable Currents,"* [arXiv:2202.02064](https://arxiv.org/abs/2202.02064).
- [68] R. Elber, *Milestoning: An Efficient Approach for Atomically Detailed Simulations of Kinetics in Biophysics*, *Annu. Rev. Biophys.* **49**, 69 (2020).
- [69] C. Maes, K. Netočný, and B. Wynants, *Dynamical Fluctuations for Semi-Markov Processes*, *J. Phys. A* **42**, 365002 (2009).
- [70] M. K. Chari, *On Reversible Semi-Markov Processes*, *Operations Research Letters* **15**, 157 (1994).
- [71] V. Girardin and N. Limnios, *On the Entropy for Semi-Markov Processes*, *J. Appl. Probab.* **40**, 1060 (2003).
- [72] M. Esposito and K. Lindenberg, *Continuous-Time Random Walk for Open Systems: Fluctuation Theorems and Counting Statistics*, *Phys. Rev. E* **77**, 051119 (2008).
- [73] M. T. Semaan and J. P. Crutchfield, *Homeostatic and Adaptive Energetics: Nonequilibrium Fluctuations beyond Detailed Balance in Voltage-Gated Ion Channels*, [arXiv:2202.13038](https://arxiv.org/abs/2202.13038).
- [74] D. Andrieux and P. Gaspard, *The Fluctuation Theorem for Currents in Semi-Markov Processes*, *J. Stat. Mech.* (2008) P11007.
- [75] D. T. Gillespie, *Exact Stochastic Simulation of Coupled Chemical Reactions*, *J. Phys. Chem.* **81**, 2340 (1977).
- [76] K. Sekimoto, *Derivation of the First Passage Time Distribution for Markovian Process on Discrete Network*, [arXiv:2110.02216](https://arxiv.org/abs/2110.02216).
- [77] T. M. Cover and J. A. Thomas, *Elements of Information Theory* (Wiley Series in Telecommunications and Signal Processing) (Wiley-Interscience, New York, 2006).
- [78] A. Gomez-Marin, J. M. R. Parrondo, and C. Van den Broeck, *Lower Bounds on Dissipation upon Coarse Graining*, *Phys. Rev. E* **78**, 011107 (2008).